JGR Oceans

RESEARCH ARTICLE
10.1029/2019JC015643

Special Section:
Contributions from the Physics of Estuaries and Coastal Seas meeting, 2018

Modeling Mud and Sand Transfers Between a Macrotidal Estuary and the Continental Shelf: Influence of the Sediment Transport Parameterization

M. Diaz[1], F. Grasso[1], P. Le Hir[1], A. Sottolichio[2], M. Caillaud[1], and B. Thouvenin[1]

[1]IFREMER - DYNECO/DHYSED, Plouzané, France, [2]University of Bordeaux, EPOC, Pessac, France

Abstract Coastal environments are directly influenced by terrigenous inputs coming from rivers through estuaries. Quantifying the amount of nutrients and contaminants transported by sediments from continental areas to the sea is crucial for marine resources protection. However, the complexity of estuarine dynamics makes it difficult to quantify sediment fluxes from field measurements alone and requires numerical modeling. Thus, using a realistic 3-D hydrodynamic and sediment transport model, this study aims at evaluating the influence of model empirical parameters on sediment fluxes and estimating uncertainties on mud and sand transfers at a macrotidal estuary mouth. A sensitivity analysis, considering changes in sediment transport parameters, revealed that the system is sensitive not only to settling and erosion parameterizations but also to the spin-up period and the sediment sliding process. Both estuarine circulation and tidal pumping induce a residual up-estuary transport, which is balanced by seaward export during spring tides. Although more fine sediments are exported within the surface turbid plume during high river discharge, the net mud transport is directed up-estuary due to increased baroclinic circulation. Besides, model results highlighted a strong seasonal variability in sediment fluxes with a short and high import during high river flow and a long and weak export during low river flow. Uncertainties associated with the simulated fluxes were about 93% for mud and 51% for noncohesive classes, based on the best performing parameter sets for surface suspended sediment concentrations. These results can be reliably extrapolated to similar macrotidal estuarine systems.

Plain Language Summary Estuaries are transitional zones between terrestrial and marine environments (freshwater vs. saltwater). Because of their potential to transport nutrients and contaminants, quantifying the amount of sediment particles (mud and sand) exchanged at this interfacial area is essential for marine resources protection. Here, we use a realistic numerical model of sediment transport applied to an estuary and its adjacent continental shelf. Some parameters in the model are not well known and require calibration. This study aims at evaluating the impact of various model calibrations on simulated sediment exchanges at the estuary mouth. We found that the simulated sediment behavior is very sensitive to the selected model parameters. The quantity and direction of simulated exchanges are influenced by the parameterization of sediment erosion and settling (i.e., the rate at which particles are suspended and settle out). The dominant physical processes driving these exchanges are strongly influenced by river flow and tide amplitude. Sediment transfers are very intense and directed upstream during a short period in winter and compensated by weak export seaward during a long period in summer. Besides, uncertainties associated with simulated sediment exchanges are about 93% for mud and 51% for sands, which can reliably be applied to similar estuarine systems.

Key Points:
- A 3-D process-based model is used to study sediment fluxes sensitivity to sediment transport parameters along an estuary-shelf system
- Besides erosion and settling parameterizations, sediment fluxes are notably sensitive to sediment sliding process and spin-up period
- For equifinal parameter sets, uncertainties associated with sediment fluxes at the estuary mouth can reach 93% for mud and 51% for sands

Correspondence to:
M. Diaz,
melanie.diaz29@hotmail.com

Citation:
Diaz, M., Grasso, F., Le Hir, P., Sottolichio, A., Caillaud, M., & Thouvenin, B. (2020). Modeling mud and sand transfers between a macrotidal estuary and the continental shelf: Influence of the sediment transport parameterization. *Journal of Geophysical Research: Oceans*, *125*, e2019JC015643. https://doi.org/10.1029/2019JC015643

Received 11 SEP 2019
Accepted 18 MAR 2020
Accepted article online 24 MAR 2020

1. Introduction

Many ecological and physicochemical processes take place in estuaries (Chapman & Wang, 2001; Ridgway & Shimmield, 2002), which makes them complex; dynamic; and, above all, crucial environments for the ecology, biology, and other biogeochemical functioning of the coastal ocean. During their transfer from continental areas to the sea, pollutants, such as heavy metals and radionuclides, can be adsorbed by fine suspended particles and trapped in sediments in the estuary or exported to the sea. As estuaries are among the most productive marine ecosystems in the world (Morris et al., 1978; Underwood & Kromkamp, 1999), investigating estuarine sediment dynamics is of major interest for the protection of coastal and estuarine resources, as well as for economic stakes (McSweeney et al., 2017).

Because of the influence of both tide and river regimes in tide-dominated estuaries, the transport of particles is governed by complex processes involving hydrodynamics, hydrology, and sediment dynamics (Burchard & Baumert, 1998). The interaction between river discharge, gravitational circulation, and tidal pumping induces an accumulation of suspended sediment in an Estuarine Turbidity Maximum (ETM) (Allen et al., 1977; Burchard et al., 2018; Festa & Hansen, 1978; Geyer, 1993; Scully & Friedrichs, 2007). In these environments characterized by high turbidity levels and intricate sediment dynamics, particle contamination by pollutants can have severe implications for ecology and biology (Roberts, 2012).

The residence time of sediments within an estuary and the net sediment fluxes to the open sea, which are strongly influenced by both the ETM and the river flow dynamics, are key parameters to better understand the fate of contaminants and to protect coastal resources. Due to the broad range of spatial and time scales involved, quantifying sediment fluxes between the estuary and the adjacent continental shelf is challenging, and only few studies have investigated their seasonal and annual variability (Dyer, 1989). Schulz et al. (2018) summarized the various methods generally used to investigate such quantities. Approaches based on field data are challenging to implement due to the cost in time and money to collect sufficiently accurate measurements (Sommerfield & Wong, 2011). An alternative method for assessing sedimentary fluxes, as proposed by Doxaran et al. (2009), combines in-situ measurements with ocean color satellite data. It enables to overcome the constraints of space, but its applicability is often limited in estuarine environment because of the limitations of calibration algorithms and the low temporal discretization. Besides, it only provides information about the surface layer, which is not sufficient to quantify sediment fluxes accurately over the whole water column. Therefore, as proposed by Schulz et al. (2018), one of the most appropriate ways to quantify suspended sediment fluxes is to use validated numerical models.

Numerical hydrodynamic and sediment transport models provide a strong scientific basis for improving our understanding of estuarine and coastal sediment dynamics. Merritt et al. (2003), followed by Aksoy and Kavvas (2005), reviewed the different types of models used to simulate sediment transport: empirical or statistical (Wischmeier & Smith, 1978), conceptual (Viney & Sivapalan, 1999), and physics-based models. The differences mainly arise from the physical processes considered, the algorithms used to describe the physical processes, and the conditions for which the model was developed. Physics-based models, also called process-based models, solve the fundamental physical equations of mass and momentum conservation for flow and mass conservation for sediment. They differ from one another in terms of complexity, ranging from exploratory (Dijkstra et al., 2019; Huijts et al., 2006) to complex models, which aim is to reproduce real-life systems as accurately as possible.

With growing computational ability and facilities, process-based models are becoming increasingly exhaustive in terms of computed physical processes. About sediment transport models in particular, recent efforts have focused on developing mixed sediment (mud/sand) transport models taking into account erosion, deposition and consolidation processes in a two or multilayered sediment compartment (Bi & Toorman, 2015; Grasso et al., 2015; Le Hir et al., 2011; Sanford, 2008; Sherwood et al., 2018; van Kessel et al., 2011). However, these realistic complex process-based models still need to be calibrated by adjusting several independent empirical parameters (Murray et al., 2016). As argued by van Maren and Cronin (2016), the higher the complexity of a model, the higher the computational cost of model runs. This implies that the number of simulations that can be carried out within a reasonable framework is often limited and stochastic simulations are not possible. Besides, due to the number of parameters involved, the calibration process requires a lot of in-situ measurements under different conditions. As French (2010) points out, given the cost and difficulty of collecting data in the field, their quantity and quality often do not match the broad range of complex physical processes considered. In addition, the calibration phase is based on comparisons of modeled and observed time series at a few specific locations, not always coinciding with the purpose of the study in terms of considered area or parameters. In some circumstances, this allows several empirical parameter values to perform equally well compared to the measured data. Therefore, it is challenging to evaluate the performance of models for several sets of parameters and to discriminate the "best fit."

An inaccurate quantification of hydrodynamic and sediment transport key parameters leads to epistemic uncertainty (Roy & Oberkampf, 2011; van Maren & Cronin, 2016). Van Maren and Cronin (2016) investigated the effect of *equifinality* on predictive model capacities. Equifinal parameter sets are defined as different combinations of parametric values that can reproduce observational data equally well (Beven, 1993) and

are mainly caused either by a lack of validation data or by redundant model parameters. Using a complex 3-D process-based model, van Maren and Cronin (2016) explained that stochastic simulations are inappropriate not only because of the required computational cost but also because of the interdependence of the input parameters. A random distribution of their values would result in physically meaningless parameter sets and, therefore, irrelevant model outcomes. Therefore, they proposed a methodology consisting of studying a limited number of equifinal calibration sets, each with similar performance when compared to suspended sediment concentration (SSC) field measurements, in order to evaluate the impact of equifinality on suspended sediment dynamics. Given that the only available measurement data for calibration are often limited to SSC measurements, the validation of sediment transport models is frequently based solely on simulated and measured SSC comparisons. Thus, properly calibrating models and quantifying uncertainties for the estimation of sediment budgets remains a challenging issue. Therefore, the proposed methodology hereafter is to investigate the impact of equifinality, identified during the calibration process, on simulated sediment fluxes.

Based on a realistic 3-D process-based numerical model of the Gironde Estuary (France), this study aims at estimating the influence of sediment transport parameters on sediment fluxes between a macrotidal estuary and the adjacent continental shelf. Particularly, one of the key objectives is to quantify uncertainties on mud and sand transfers along the land-sea continuum (i.e., river catchment to open sea). The Gironde Estuary is one of the largest estuaries in Europe and is characterized by a well-developed turbidity maximum, with surface SSC up to a few $kg.m^{-3}$ (Castaing & Allen, 1981; Doxaran et al., 2009; van Maanen & Sottolichio, 2018). It is a partially mixed to well-mixed macrotidal estuary with a strong river discharge influenced by a pronounced seasonal variability. The implemented hydrodynamic model is coupled to a multilayer mud and sand transport module that takes into account advection, diffusion, and consolidation processes and is forced by realistic boundary conditions (tide, wind, waves, river flow, and meteorological surges). Most of the estuarine sediment transport processes and patterns are found in this estuary and are simulated by the implemented process-based model implemented.

To reach the objectives of this study, a sensitivity analysis of the sediment fluxes at the mouth of the estuary is applied considering changes in key sediment parameters. Following the methodology proposed by van Maren and Cronin (2016), a sensitivity analysis is first carried out to identify which key sediment parameters contribute the most to output variations and perform the best in terms of SSC dynamics. Due to the computational cost of running the model (2-year simulations), a single-parameter perturbation approach was used, where parameters were varied in a range of physically meaningful values. Model performances were then calculated in order to define equifinal parameter sets. Finally, the sensitivity of simulated fluxes through a section is investigated, and especially the sensitivity to previously defined equifinal parameter sets, in order to evaluate the corresponding uncertainties on computed sediment fluxes. The study area and numerical modeling setup are described in section 2 as well as the strategy established for the sensitivity analysis. Section 3 describes model results in terms of hydrodynamics and hydrology, as well as the sensitivity of SSC to sediment model key parameters. Finally, the sensitivity of sediment fluxes between the estuary and the continental shelf to the various sets of parameters is presented in section 4.

2. Methods

2.1. Study Area

The Gironde Estuary has a total surface area of 635 km^2 (Jalon-Rojas et al., 2015). It is located in the Bay of Biscay in the southwest of France (Figure 1) and drains a watershed of about 71,000 km^2 (Allen et al., 1980; Fuentes-Cid et al., 2014; Savoye et al., 2012). The estuary has a regular funnel shape extending over about 75 km from the mouth to the junction of the Garonne and Dordogne tidal rivers. The tide propagates in the river as far as 170 km from the mouth. The yearly-averaged total river discharge of both the Garonne and Dordogne rivers is about 700 $m^3.s^{-1}$ (Jalon-Rojas et al., 2015). The Garonne River is the main tributary, supplying about 60% of freshwater and 70% of the suspended sediments to the estuary, while the Dordogne River provides the rest (Parra et al., 1999; Schäfer et al., 2002). A clear river flow seasonality is observed for the Garonne and Dordogne regimes combined, a flood period from November to May (maximum monthly mean values of 1,500 $m^3.s^{-1}$, usually in January) and a low flow period from June to October (less than 200 $m^3.s^{-1}$ in August). It is one of the two main estuaries of the French Atlantic coast flowing into the Bay of Biscay

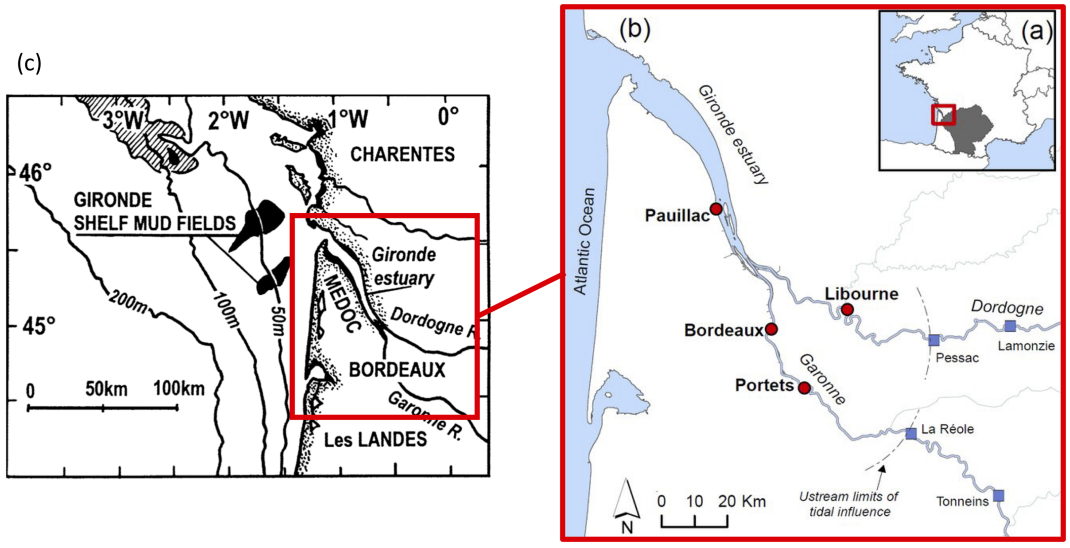

Figure 1. The Gironde fluvial-estuarine system: (a) location map. The gray area indicates the watershed of the Garonne and Dordogne rivers; (b) the estuary and its main tributaries. Red circles indicate the MAGEST stations (see section 3); blue squares indicate the hydrometric stations. (c) Location map of muddy patches (Gironde shelf mud fields in black) on the continental shelf of the Bay of Biscay, France. The gray area represents an extended muddy sand patch. Figures were modified from Lesueur et al. (2002) and Jalon-Rojas et al. (2015).

(Jouanneau et al., 1999). The riverine sediment supply from the Gironde Estuary to the continental shelf is about 1.5×10^6 t.year^{-1} and is estimated to contribute 60% of fine sediment input into the Bay of Biscay (Jouanneau et al., 1999).

The Gironde estuarine system is macrotidal, with tides at the mouth ranging on average from 1.5 m during neap tides to 5.5 m during spring tides (Castaing & Allen, 1981). Following the classification of Le Floch (1961), the Gironde is considered hypersynchronous (Allen et al., 1980). This means that the tidal wave amplitude reaches a maximum in the estuary, where a balance occurs between the amplification due to cross-section reduction and the attenuation due to bottom friction. Hydrodynamics are strongly influenced by asymmetrical tidal currents as well. Large amounts of mud are resuspended during peak tidal currents, particularly during flood, and rapid settling occurs during the following high-water slack, resulting in upstream sediment tidal pumping (Allen et al., 1980; Castaing & Allen, 1981; Uncles et al., 1985).

The combination of gravitational circulation, tidal asymmetry mixing, and tidal pumping generates one of the most developed and concentrated ETM in Europe, with more than 1 kg.m^{-3} SSC in surface waters (Castaing & Allen, 1981; Doxaran et al., 2009) and an estimated ETM mass of 4 to 6 Mt during spring tides (Allen et al., 1977; Jouanneau, 1979; van Maanen & Sottolichio, 2018). The seasonal variability in suspended sediment concentration is particularly high with bottom values ranging from less than 0.1 up to a few kg.m^{-3} (Sottolichio & Castaing, 1999). The longitudinal location of the ETM in the estuary depends on the seasonal dynamics of the river flow and changes in salinity intrusion (Allen et al., 1980; Jalon-Rojas et al., 2015; Sottolichio et al., 2000). During high river flow, the density gradient is well developed, and the ETM is located at the density node (Allen et al., 1980). During periods of low river flow, the ETM stretches upstream over up to 40 km to reach Portets on the Garonne River and Libourne on the Dordogne River (Figure 1b). The deepest and broadest parts of the channel, where the ETM occurs, are likely to trap large quantities of fine particles. This particulate matter forms highly concentrated benthic suspensions, resulting in thick layers of fluid mud, with concentrations up to 300 kg.m^{-3} (Allen, 1971). A secondary stable turbidity maximum was observed in the middle of the estuary (near Pauillac; Figure 1b) and is induced by a very dynamic zone often referred to as the "erosion maximum zone" (Allen et al., 1980; Doxaran et al., 2009; Sottolichio & Castaing, 1999). The enhanced deposition occurring at this site has been linked to the presence of a narrow deep pit in the axis of the channel. This feature acts as a permanent source of easily erodible mud, which maintains the secondary peak of turbidity (Sottolichio & Castaing, 1999).

The surficial sediment map also shows the presence of two mud fields off the Gironde Estuary mouth, on the continental shelf (Figure 1c; Lesueur et al., 1996). The largest (420 km^2) is called the "West-Gironde Mud Patch" (WGMP) and is located about 30 km west of the mouth. The second (50 km^2) is observed south of the WGMP and is referred to as the "South-Gironde Mud Patch" (SGMP). Both are located in front of the two channels of the Gironde mouth, at intermediate depths between 30 and 75 m deep. Most of the particles contributing to these muddy patches originate from the Gironde watershed (Lesueur et al., 2002), indicating that fine particles can accumulate in these areas when flowing out of the estuary.

2.2. Numerical Model Setup

2.2.1. Hydrodynamic Model

For studying sediment transport in the Gironde Estuary and on the continental shelf, a 3-D numerical model was developed, based on the MARS3D model (Lazure & Dumas, 2008). It solves the momentum equations using a finite difference scheme under the Boussinesq and hydrostatic hypotheses.

The model grid covers the Gironde Estuary and its tributaries, from the upper limit of tidal influence (La Réole in the Garonne River and Pessac in the Dordogne River) out to about the 100-m isobath offshore, and from the Arcachon basin in the south to Les Sables-d'Olonne in the north (Figure 2). An orthogonal curvilinear grid was implemented to better account for the complex shape of the estuarine mouth, the river meanders, and the Marennes-Oléron system. The smallest computational cells are located upstream in rivers and are approximately 40 × 350 m, while offshore cells measure up to 2 km × 2 km. The grid contains over 400 × 220 cells along the west-east and south-north directions, respectively. The vertical grid was discretized in 10 equidistant sigma layers across the water column.

The circulation was forced at the open boundaries (west and south) using the main tidal components. The model was also forced using wind stresses and pressure gradients provided by the high-resolution meteorological AROME model (Meteo-France). Surges at the open boundaries were provided by a configuration of the MARS2D numerical model applied to a larger domain. The realistic Garonne, Dordogne, and Charente river flows were prescribed at La Réole, Pessac, and Rochefort, respectively (Figure 1b). Waves were simulated using the WAVEWATCH III® (WW3) numerical model on the same computational grid as the circulation model (Roland & Ardhuin, 2014). The wave model was forced using the free surface elevation and current velocity provided by the hydrodynamic model MARS3D, as well as local winds and, at the shelf boundary, the swell data extracted from a larger Atlantic Ocean model. The total bed skin shear stress was expressed as a combination of the current and wave-induced bed shear stresses (Soulsby, 1997) as described in detail by Grasso et al. (2018) and Appendix A.

2.2.2. Sediment Transport Model

The hydrodynamic model was coupled with the process-based multiclass, multilayer sediment transport module MUSTANG (MUd and Sand TrANsport modeling) described by Le Hir et al. (2011), Grasso et al. (2015), and Mengual et al. (2017). The sediment transport module computes the spatial and temporal variations of sand and mud mixtures under the effect of hydrodynamic forcing, including the combined action of current and waves. In the water column, it solves the advection-diffusion equations for different particle classes (in a 3-D framework for mud, depth-averaged for sands) as well as sediment exchanges at the bed interface through erosion and deposition processes. It also simulates the bed sedimentation and consolidation processes.

In this study, five representative sediment classes were chosen based on the granulometry data available for the Gironde Estuary and the adjacent continental shelf: gravel (diameter $d = 3$ mm), three sizes of sands (medium sand $d = 400$ μm, fine sand $d = 250$ μm, and very fine sand $d = 100$ μm), and mud ($d = 30$ μm). For each class, the grain density was 2,600 $kg.m^{-3}$. The initial distribution of sediment classes over the domain was considered uniform with 10% of gravel, 20% of each sand class and 30% of mud. The initial sediment bed had a uniform thickness of 3.67 m, which followed a model adjustment based on the initial sediment concentration, the sediment class fractions, and a bed porosity of 0.61.

The river sediment supplies were pure mud and are forced upstream at the same location as river flows. Concentrations were dependent on the water discharge, following Coynel (2005) for the Garonne and Dordogne rivers, and were imposed at a constant value of 0.05 $kg.m^{-3}$ for the Charente River.

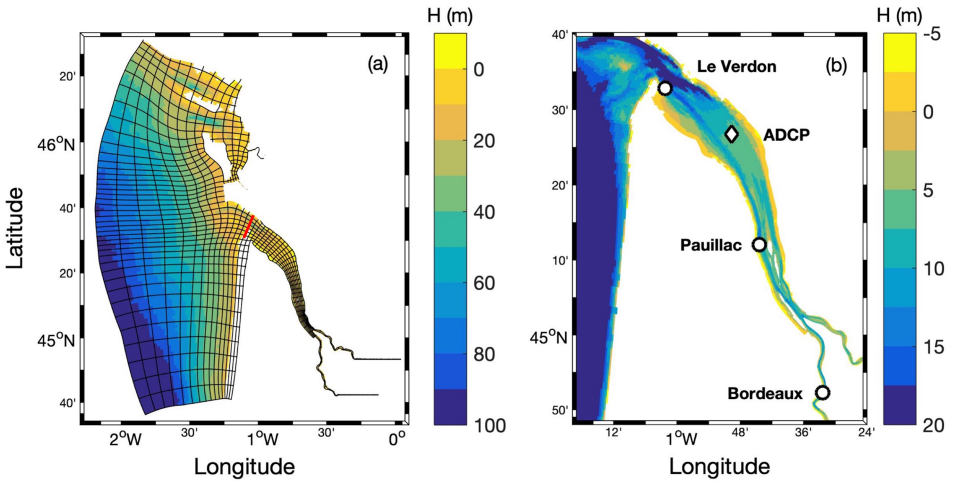

Figure 2. (a) Geographic extent of the 3-D model configuration with its bathymetry (mean sea level chart datum). The black lines represent the mesh grid (every fifth cell). The red line illustrates the cross section where the sediment fluxes were calculated. (b) A zoom on the estuary and its bathymetry. The white circles indicate the points where water level, salinity, and SSCs were measured (only water level measurements are available at Le Verdon), and the white diamond represents the ADCP location.

2.2.2.1. Settling

Non-cohesive classes (gravel and sands) had fixed settling velocities depending on their diameters (Soulsby, 1997). Their advection, computed as depth averaged, is corrected using a logarithmic vertical profile of current and a "Rouse" vertical profile of concentration (Waeles et al., 2007). The mud class was defined as a three-dimensional variable with a settling velocity $w_{s,mud}$ varying in time and space following van Leussen (1994):

$$w_{s,mud0} = \min\left[\boldsymbol{w_{s,max}}, \max\left(\boldsymbol{w_{s,min}}, \boldsymbol{c_1} C_{mud}^{\boldsymbol{c_2}} \frac{1+\boldsymbol{a}G}{1+\boldsymbol{b}G^2}\right)\right], \tag{1}$$

with C_{mud} the mud concentration, G the turbulent shear rate, and a, b, c_1, and c_2 the calibration parameters. $w_{s,mud0}$ was limited by minimum and maximum values ($w_{s,min}$ and $w_{s,max}$). Such a formulation makes it possible to account for flocculation processes, thus increasing the mud settling velocity when the mud concentration in the water column increases (see Appendix C, Figure C1a). The equation also considers the turbulence effects on flocs: small turbulence increases the flocculation process, whereas larger turbulence tends to disaggregate flocs and reduce the settling velocity (Figure C1b).

To account for the influence of salinity on flocculation, a dependency between the mud settling velocity and salinity (S) was computed (Migniot, 1968; Mikes et al., 2004; Thill et al., 2001). This effect was previously accounted for by Lajaunie-Salla et al. (2017) in the Gironde estuarine system and largely contributed to simulate high SSC levels and maintain the ETM in the tidal rivers. A critical salinity S_{cr} of 5 psu was chosen, below which settling velocity decreases with salinity, as follows:

$$w_{s,mud} = \begin{cases} w_{s,mud0}, & if\ S \geq S_{cr} \\ \max\left(w_{s,min}, \dfrac{S^* w_{s,mud0}}{S_{cr}}\right), & if\ S < S_{cr} \end{cases}. \tag{2}$$

The deposition flux D_i for each sediment class i was calculated using a critical shear stress for deposition $\tau_{d,i}$. The general formulation follows the law of Krone (1962) as described in Le Hir et al. (2011), Mengual et al. (2017), and Grasso et al. (2018). In Krone's law, the deposition flux is modulated by a factor that takes into account the ratio between the local bed shear stress and $\tau_{d,i}$. This factor can be considered as a mean of representing a "deposition efficiency," as proposed by Winterwerp et al. (2018). In the present study, in order to reduce computational cost, the concentration of the muddy fresh deposit was set at 100 kg.m^{-3}, and $\tau_{d,i}$

was considered an intermediate value (i.e., for mud: 5 Pa), thus preventing deposition when the bottom shear stress exceeds this threshold.

2.2.2.2. Erosion

The erosion flux was based on the Partheniades-Ariathurai equation (Partheniades, 1965), which calculates an erosion flux only when the bottom shear stress exceeds the critical erosion stress:

$$\begin{cases} \tau > \tau_{ce} \Rightarrow E = E_0 \left(\frac{\tau}{\tau_{ce}} - 1 \right)^n \\ \tau < \tau_{ce} \Rightarrow E = 0 \end{cases}, \quad (3)$$

with E the erosion flux, E_0 an erodibility parameter (expressed in $kg.m^{-2}.s^{-1}$), τ_{ce} the critical shear stress for erosion ($N.m^{-2}$), and n a calibration parameter. In the case of mixed sediments, a distinction between cohesive and noncohesive sediment behaviors was made depending on the mud fraction (Le Hir et al., 2011; Sherwood et al., 2018; Waeles et al., 2007). Therefore, the erosion-related parameters (i.e., E_0, τ_{ce}, and n) were set at different values depending on the mass fraction of mud in the surficial layer (f_m). Further details regarding the parameterization of the erosion law for both cohesive and noncohesive behaviors, as well as details on the transition between them, can be found in Appendix B.

2.2.2.3. Miscellaneous

Consolidation was simulated using solving Gibson's equation for mixed sediments (Grasso et al., 2015) allowing a dependency between the critical bed shear stress and the state of consolidation (equation B2 in Appendix B). Note that a similar model setup (i.e., MARS3D, WW3, and MUSTANG) was implemented for the macrotidal Seine Estuary (France) and provided reliable simulations of suspended sediment dynamics at time scales ranging from the duration of a tidal cycle to several years (Grasso et al., 2018; Schulz et al., 2018). Moreover, a morphostatic approach was considered (i.e., no feedback between the evolution of bathymetry and hydrodynamics), which proved reliable for short time scales of a few years (Grasso & Le Hir, 2019).

The calculation of sediment fluxes between continental and marine areas was performed for every time step during the simulation to ensure the conservation of sediment mass (Schulz et al., 2018). It should be noted that the present study does not account for dredging activities. Because more than 90% of the dredged material is dumped in the estuary, it was assumed that it does not significantly influence residual sediment fluxes at the mouth.

2.3. Strategy to Assess the Model Sensitivity to Independent Key Parameters

Due to the lack of field measurements, many of the calibration parameters in a sediment transport model are based either on estimated values from previous studies or a best fit evaluation of simulated SSCs compared to field data for a range of "physically valid" values. A total of 29 model experiments (noted T1 to T29) were carried out to assess the influence of sediment transport parameterization on suspended sediment dynamics and fluxes. The main sediment transport model parameters were individually varied in a range of acceptable values. The following sections provide an overview of the values tested for the main calibration parameters (mud settling velocity, erosion law, and additional parameters). The parameters were first adjusted one by one, except for some tests specified in section 2.3.3.4 and Table 1. The model performances were then estimated for each simulation based on comparisons between simulated and observed SSC data within the estuary. Standard statistical metrics were used to provide a classification of model runs as follows: "bad performers," "good performers," and "very good performers." Each category can be considered as "equifinal" parameter sets as they perform almost equally well compared to measurements. The sensitivity of simulated sediment fluxes for each category was studied in order to quantify uncertainties based on the model's ability to reproduce SSC levels. Hereafter are briefly described the values of the parameters tested in the 29 model experiments (summarized in Table 1 and detailed in Appendices C to E).

2.3.1. Mud Settling Velocity

Mud settling velocity is one of the essential calibration parameters for muddy sediments (Brenon & Le Hir, 1999; French, 2010; van Maanen & Sottolichio, 2018). A baseline parameterization for mud settling velocity (WS1) was calculated following the Van Leussen's formulation (equation 1) with calibrated parameters from Grasso et al. (2018) (see Table C1 in Appendix C). The "baseline parameterization" does not correspond to the best set of parameters after calibration but is the one used in all the tests from which the parameters were modified to study the model sensitivity. Besides, the dependence of the mud settling velocity on salinity

Table 1
Sediment Model Parameters and Performances for the 29 Simulations

Test	Mud setting velocity	$E_{0,mud}$	$E_{0,sand}$	Transition	Sliding effect (%)	$z_{0,sed}$ (m)	Other param.	B* Pau.	RMSE* Pau.	RMSE Pau.
T1	WS1	Em1	Es,ero	Linear	0	1×10^{-5}	/	−0.35	−0.77	0.85
T2	**$WS1_{max,1}$**	**Em3**	Es,ero	Linear	0	1×10^{-5}	/	−0.29	−0.77	0.82
T3	**$WS1_{max,2}$**	**Em6**	Es,ero	Linear	0	1×10^{-5}	/	−0.71	−0.76	1.04
T4	**$WS1_{min}$**	**Em3**	Es,ero	Linear	0	1×10^{-5}	/	−1.02	−0.76	1.27
T5	**WS2**	**Em6**	Es,ero	Linear	0	1×10^{-5}	/	−0.66	−0.76	1.00
T6	**WS3**	**Em6**	Es,ero	Linear	0	1×10^{-5}	/	−0.62	−0.77	0.99
T7	**WS4**	**Em6**	Es,ero	Linear	0	1×10^{-5}	/	−0.64	−0.76	0.99
T8	**WS5**	**Em6**	Es,ero	Linear	0	1×10^{-5}	/	−0.33	−0.77	0.83
T9	**WS6**	**Em6**	Es,ero	Linear	0	1×10^{-5}	/	−0.70	−0.77	1.04
T10	WS1	**Em2**	Es,ero	Linear	0	1×10^{-5}	/	−0.25	−0.77	0.81
T11	WS1	**Em3**	Es,ero	Linear	0	1×10^{-5}	/	−0.41	−0.78	0.88
T12	WS1	**Em4**	Es,ero	Linear	0	1×10^{-5}	/	−0.69	−0.76	1.03
T13	WS1	**Em5**	Es,ero	Linear	0	1×10^{-5}	/	−0.79	−0.77	1.10
T14	WS1	**Em6**	Es,ero	Linear	0	1×10^{-5}	/	−0.64	−0.76	0.99
T15	WS1	**Em7**	Es,ero	Linear	0	1×10^{-5}	/	−0.76	−0.77	1.08
T16	WS1	Em1	**Es,VR84**	Linear	0	1×10^{-5}	/	−1.11	−0.77	1.35
T17	WS1	Em1	**Es,ero10**	Linear	0	1×10^{-5}	/	0.33	−0.93	0.98
T18	WS1	Em1	Es,ero	**Exp40**	0	1×10^{-5}	/	−0.82	−0.75	1.12
T19	WS1	Em1	Es,ero	**Lin. + f_{mcr1} max 20%**	0	1×10^{-5}	/	−0.35	−0.77	0.84
T20	WS1	Em1	Es,ero	**Exp40 + f_{mcr1} max 20%**	0	1×10^{-5}	/	−0.86	−0.76	1.15
T21	WS1	Em1	**Es,ero10**	**Exp40**	0	1×10^{-5}	/	−0.38	−0.79	0.88
T22	WS1	Em1	Es,ero	Linear	**15**	1×10^{-5}	/	−0.19	−0.78	0.81
T23	WS1	Em1	Es,ero	Linear	**30**	1×10^{-5}	/	−0.15	−0.79	0.80
T24	WS1	Em1	Es,ero	Linear	**50**	1×10^{-5}	/	−0.15	−0.81	0.82
T25	WS1	Em1	Es,ero	Linear	**100**	1×10^{-5}	/	−0.19	−0.82	0.84
T26	WS1	Em1	Es,ero	Linear	0	**5×10^{-5}**	/	−0.52	−0.76	0.92
T27	WS1	Em1	Es,ero	Linear	0	**Spat.**	/	−0.74	−0.76	1.06
T28	WS1	Em1	Es,ero	Linear	0	1×10^{-5}	**Initial deposited fluid mud**	−0.34	−0.77	0.84
T29	WS1	Em1	Es,ero	Linear	0	1×10^{-5}	**20 vertical layers**	−0.24	−0.78	0.82

Note. Terms in bold are those that differ from the baseline paremeterization.

(see section 2.2.2) was applied to all tests, but its contribution to simulated sediment concentrations and fluxes was not studied in this paper.

The sensitivity of the model to the weight of the suspended mud concentration C_{mud} in the $w_{s,mud}$ equation (equation 1) was first investigated by alternatively reducing and increasing its contribution. The minimum and maximum settling velocities were also varied, and the turbulence effect on flocculation was in turn taken into account or not. All tests on mud settling velocity are described in Appendix C.

2.3.2. Erosion Law

2.3.2.1. Erosion of Noncohesive Sediment

Knowledge of sand erosion fluxes is rather poor compared to the numerous studies on the initiation of motion (critical shear stress). The Erodimetre formulation, proposed by Le Hir et al. (2008), hereafter noted "Es,ero" and described in Appendix B (equation B1), was used as baseline parameterization. In order to study the influence of the erodibility coefficient $E_{0,sand}$, the formulation from van Rijn (1984) (equation D1), denoted as "Es,VR84," was tested (Test T16, Table 1). A third test was carried out using the Erodimetre formulation multiplied by a factor 10, hereafter noted "Es,ero10" (Test T17, Table 1).

2.3.2.2. Erosion of Cohesive Sediment

Pure mud erosion parameters are mostly empirical and are among the key calibration parameters. For the present study, several values of both $E_{0,mud}$ and the mud critical shear stress for erosion were tested within a range of "acceptable" values seen in literature (see details in Appendix D).

2.3.2.3. Transitional Behavior

Two types of formulations were tested to describe the transition from noncohesive to cohesive behaviors, which depend on mud content: (i) a linear equation (baseline parameterization) and (ii) an exponential

one (Test T18) based on Mengual et al. (2017). The onset of the transitional behavior was also investigated (i.e., the value of the mud content below which pure sand erosion is prescribed) and is described in Appendix D.

2.3.3. Additional Sediment Transport Parameters

2.3.3.1. Sliding Process

As the bed slope is likely to increase with erosion and deposition processes (e.g., between depositing banks and an eroding channel), sliding of sediments along the slope may occur. This process is not taken into account in the baseline parameterization, but several tests (T22 to T25) were performed that consider various intensities of this process (see details in Appendix E).

2.3.3.2. Skin Roughness in the Bed Shear Stress Computation

In the baseline parameterization, the skin bottom roughness $z_{0,sed}$ (considered in the bed shear stress computation) was set at a uniform and constant value of 1×10^{-4} m. Two other simulations were tested: a lower constant value of 5×10^{-5} m and a spatially and time-varying formulation (see details in Appendix E).

2.3.3.3. Sediment Bed Initialization, Vertical Discretization, and Spin-Up Period

The sediment initial distribution was uniform, and a spin-up year was computed before the analysis period to let the simulated waves and currents redistribute the sediment over the domain and ensure the model relevance (Grasso et al., 2018; Schulz et al., 2018) (see Appendix G for details on the required time of spin-up). The sensitivity of SSCs and sediment fluxes to the spin-up period is discussed based on the baseline run. Moreover, another test was carried out to assess the influence of the sediment initial distribution: an initial deposited layer of fluid mud of 4 Mt, which was equivalent to the expected ETM mass and location (upstream, in the tidal rivers), was added to the baseline uniform sediment bed (test T28). Lastly, in order to save computational time, a total of 10 vertical layers in the water column was chosen. However, the influence on fluxes of varying the number of vertical layers was tested by running a simulation with 20 layers (Test T29).

2.3.3.4. Cross-Sensitivity Tests

For the purpose of this study and to better calibrate the sediment transport model, tests were performed where several parameters were adjusted simultaneously. Following recommendations by Mengual et al. (2017) and van Maren and Cronin (2016), both the exponential transitional trend and the maximum value of f_{mcr1} were modified together, as well as the sand erosion flux and the transitional trend together.

3. Hydrodynamics and Sediment Dynamics

The following numerical model results were obtained by running simulations over the year 2015, for which tidal gauge measurements, wave heights, currents, salinity, and SSC were available simultaneously in the estuary. Velocity measurements were obtained from an ADCP deployed in the lower estuary from June to November 2015 (Ross et al., 2017). Salinity and SSC measurements were collected at two locations as part of the MAGEST (MArel Gironde ESTuary) monitoring network (Jalon-Rojas et al., 2015; Schmidt et al., 2014).

3.1. Validation of the Hydrodynamic Model

3.1.1. Water Levels

To properly reproduce the sediment transport in this type of environment, it is crucial to reproduce the tidal pumping induced by the tidal asymmetry along the estuary. The validation of water levels was carried out using tide gauge records from nine stations located along the Gironde Estuary and the Garonne River (Appendix F, Figure F1). Three of them are presented in Figure 3 (see Figure 2b for exact locations).

Water levels appear well reproduced along the estuary and over the entire simulated period with a root-mean-square error (e_{rms}) of 21 cm at the estuarine mouth (Le Verdon station), 18 cm at Pauillac, and 28 cm at Bordeaux (Figure 3). Water level comparisons with all available tide gauge stations are shown in Appendix F, Figure F2. A maximum root-mean-square error (e_{rms}) of 33 cm occurred at Ambes station (Appendix F, Figures F1 and F2). It is interesting to note that this error estimate includes differences both in tidal amplitude and tidal phase, therefore providing a more accurate error quantification than the tidal range alone. The squared correlation coefficients r^2 also confirmed the correct simulation of water levels along the estuary (Figure 3) and that the main hydrodynamic processes are well captured.

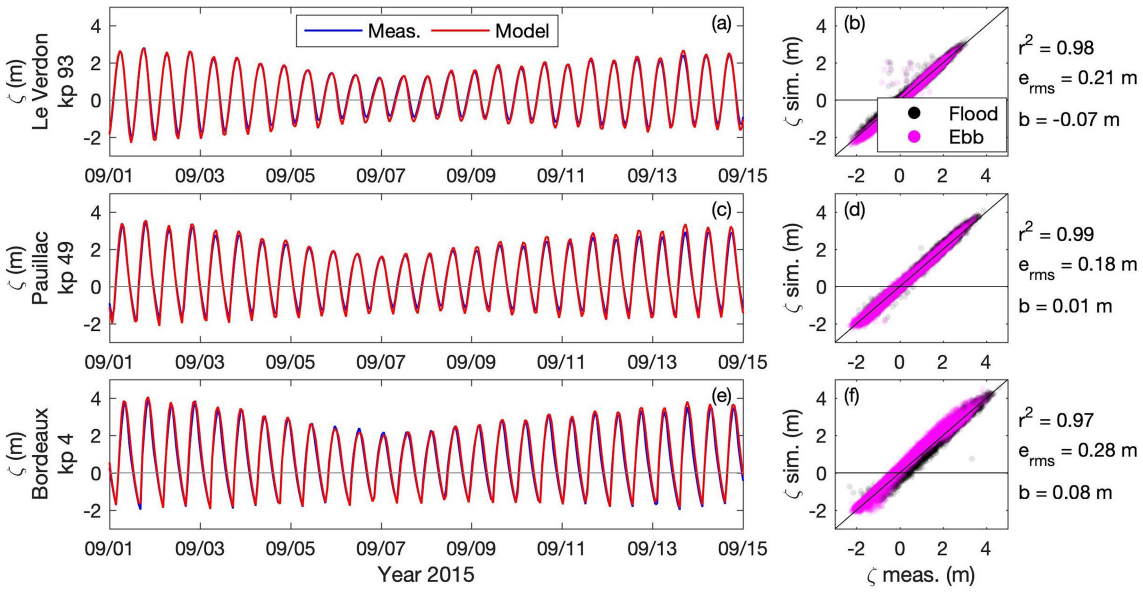

Figure 3. Water level h at (a and b) Le Verdon, (c and d) Pauillac, and (e and f) Bordeaux (see locations in Figure 2b). (Left panels) Time series of measurements (blue) and simulations (red) from 1 to 15 September 2015. (Right panels) Simulated elevations against in-situ data during flood (black dots) and ebb (pink dots) from January to December 2015, with the corresponding correlation coefficient r^2, the root-mean-square error e_{rms}, and the bias b. kp is the kilometric point associated with every station along the Gironde Estuary, with $kp = 0$ in Bordeaux.

3.1.2. Current Velocity and Direction

The validation of simulated currents was carried out using a 6-month dataset provided by an ADCP mooring located on the right bank of the lower estuary (ADCP in Figure 2b). The comparison between simulated and measured depth-averaged current intensities and directions revealed a good agreement between the model and observations (Figure 4). The model was able to simulate currents accurately ($e_{rms} \leq 0.15$ m.s^{-1} and bias $b \leq 0.08$ cm.s^{-1} for the entire sampling period) but tended to overestimate ebb current peaks during spring tides. The current vertical structure (i.e., surface and bottom velocities) was also compared and showed skills similar to the depth-averaged current (Appendix F, Figure F3).

3.1.3. Salinity

Density effects induced by salinity gradients have an important impact on the ETM development by limiting sediment export (Sottolichio et al., 2000). Data from the MAGEST monitoring network were the only available continuous measurements and were used as reference data for the validation of simulated salinities (Figure 5b).

At both Pauillac and Bordeaux stations, seasonal variations of salinity were large but well reproduced by the model (Figures 5b and 5d). At Pauillac station in the central estuary, during periods of high river flow, salinity decreases down to 0 psu, as the saline water intrusion limit is flushed toward the mouth. From May to August, when the river flow is weaker, saline waters reenter the estuary and salinity rises up to 15 psu (Figure 5b). Salinity dynamics appeared clearly influenced by the spring-neap cycle as well, which is represented by the tidal range in Figure 5a. Comparing the model output to field measurements at Pauillac station revealed a good fit ($e_{rms} = 1.5$ psu, $r^2 = 0.87$, and $b = 0.6$ psu), meaning that the model reproduces well the overall salinity dynamics in the central part of the estuary.

In the upper estuary at Bordeaux station, during periods of low river flow, the model had a tendency to overestimate the salinity (Figure 5d). In-situ data revealed an increase in salinity in late June, which was well captured by the model. However, while the measured salinity increased only as much as 1.5 psu, the model maximum salinity reached 4.5 psu, thus highlighting the lower skills of the model in this part of the estuary ($r^2 = 0.6$, $e_{rms} = 0.9$ psu). These prediction skills are sufficient for the purpose of the current study, which aims at quantifying fluxes at the mouth. The Bordeaux station is located far upstream, and the salinity variations occurring there have a negligible effect on the dynamics at the mouth.

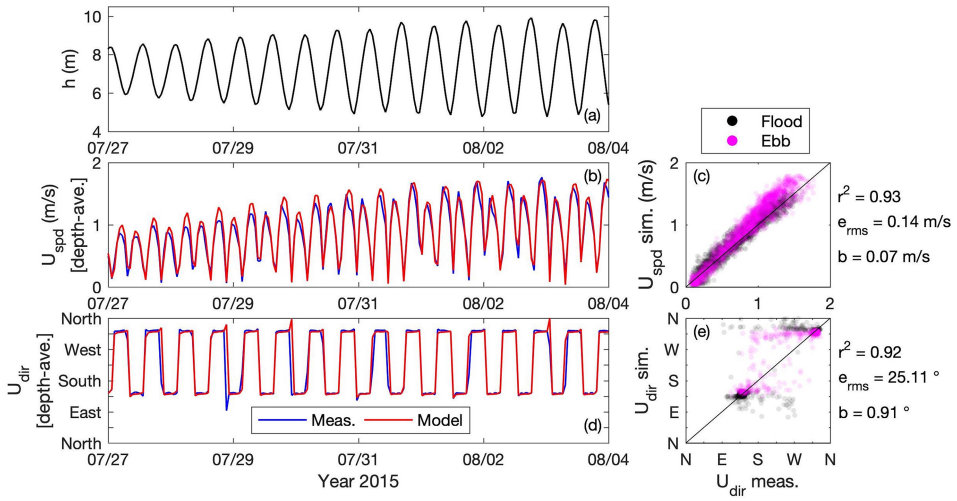

Figure 4. Comparison of observed and computed velocities at the ADCP mooring location. (a) Water level *h* simulated at the ADCP mooring location (Figure 2b). (b and c) Depth-averaged current intensity and (d and e) direction. (b and d) Time series of measurements (blue) and model outputs (red) from 27 July to 4 August 2015. (c and e) Simulated current against in-situ data during flood (black dots) and ebb (pink dots) from June to November 2015, with the squared correlation coefficient r^2, the root-mean-square error e_{rms}, and the bias *b*.

3.2. Suspended Sediment Dynamics

Field data usually available to validate sediment transport models are often limited to SSC measurements, as other field data are too expensive and difficult to collect. Remote sensing data are often not appropriate to compare with model outputs, as they are isolated in time and cannot be used to assess high-frequency dynamics in estuarine environments. In the present study, the long-term and high-frequency SSC observations available at Pauillac (central estuary) and Bordeaux (upper estuary) stations were used as SSC references.

To ensure the relevance of model analysis, the numerical modeling results presented were obtained after 1-year spin-up. This means that the final state of the first year, in terms of sediment bed composition, is used as initial bed coverage for the reference year. This allows the model to reach a (quasi)-equilibrium state by redistributing the initially uniform sediment coverage during the first year of simulation. As a consequence,

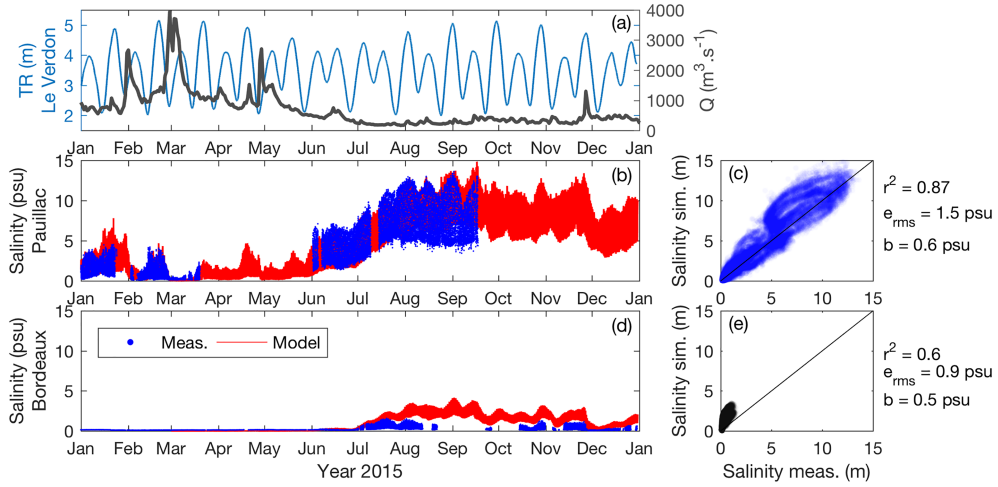

Figure 5. (a) Tidal range (TR) at the estuarine mouth (blue, Le Verdon station) and cumulated Garonne and Dordogne river flows (Q, gray) measured at La Réole and Pessac (see Figure 1 for exact locations). (b and c) Surface salinity at Pauillac and (d and e) at Bordeaux. (b and d) Time series of measurements (blue) and model outputs (red) for the year 2015. (c and e) Simulated salinity against in-situ data with the squared correlation coefficient r^2, the root-mean-square error e_{rms}, and the bias *b*.

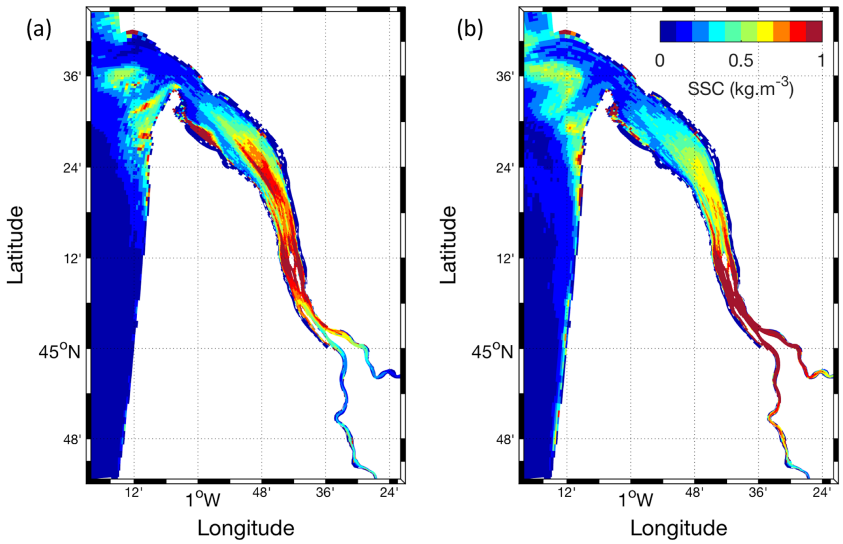

Figure 6. Near-bottom (1 m above the bed) SSC outputs for run T25 during (a) high river discharge in April 2015 and (b) low river discharge in late August 2015. A Demerliac filter was applied to model outputs and turbidity fields are shown during neap tides.

the simulation reference year starts with a bed composition that is spatially consistent with the simulated local bed shear stress. Running the model for a third realistic year after 2 years of spin-up confirmed that the equilibrium is reached after 1 year (see details in Appendix G). The model outputs of the first simulated year (the spin-up year) are shown only for comparison with the reference year for the baseline run but are generally not considered for the other simulations and are not taken into account in the final results. As well as for the hydrodynamic model, both the spin-up year and the reference year corresponded to the realistic year 2015. Model outputs were saved every hour.

The overall estuarine SSC dynamics is first discussed to ensure the reliability of model results. Test T25 (Table 1), in which the sediment sliding process was accounted for, is used in this section to illustrate the spatial and temporal SSC dynamics (Figures 6, 7, and 8). It will be seen in following results that taking this process into account allows the ETM to migrate further upstream by resuspending sediment otherwise trapped on the banks.

3.2.1. Spatial SSC Distribution

The near-bottom spatial SSC distribution was investigated during contrasted high and low river flow periods (Figure 6). A 3-day numerical filter was applied to model outputs to account for the residual suspended dynamics related to river discharge and neap-spring cycles but filtered out from semidiurnal tidal dynamics (Demerliac, 1974). SSC distributions are shown during neap conditions in order to avoid local resuspension due to strong currents during spring tides and to better illustrate the ETM location. The simulated turbidity maximum zone (TMZ) moves upstream and downstream with river flow. As previously noted by van Maanen and Sottolichio (2018), a stable ETM can be seen near the estuarine islands (latitude 45°10′N), and the dynamic ETM position translates upstream and downstream of this area. During low river flow, it extends upstream to Bordeaux in the Garonne River (Figure 6b). As soon as the freshwater discharge increases, the river's SSC levels decrease, and the TMZ moves downstream toward the estuarine mouth.

3.2.2. Estuarine Suspended Sediment Mass Dynamics

The total (depth-integrated) suspended sediment mass within the estuary, from the mouth (represented by the red line in Figure 2a) to the upstream limit of tidal influence (a few cells downstream of the domain boundary), is strongly influenced by spring-neap variations. It increases during spring tides, thus illustrating the influence of tidal currents on sediment erosion (Figure 7). During the spin-up year, a large amount of sediment is suspended and partly exported or laterally trapped (blue line, Figure 7b). This process is emphasized by larger tidal ranges occurring in February–March and September–October, during which tidal currents are stronger and promote resuspension. The second simulated year (i.e., reference year) shows more stable mass values with less than 1.5 Mt suspended mass difference between high and low river flows

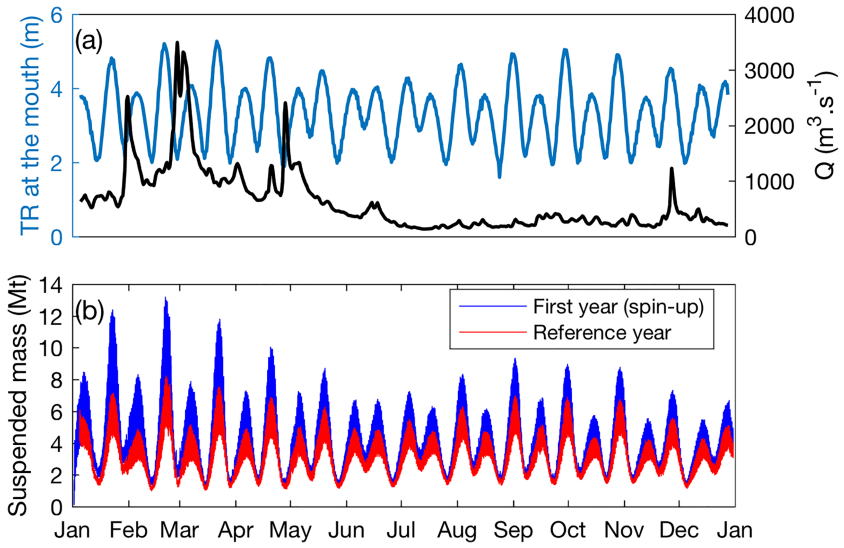

Figure 7. (a) Time series of tidal range at the estuarine mouth (blue line and left axis, Le Verdon station) and cumulated Garonne and Dordogne river flows Q (black line and right axis). (b) Time series of total suspended sediment mass in the estuary expressed in thousands of tons, for 2 years of simulation (blue line: first simulated year, referred to as the "spin-up year"; red line: second simulated year, after 1 year of spin-up, referred to as the "reference year").

during spring tide compared to an overall decrease of 4 Mt during the first simulated year. For both years, a decrease in suspended mass occurs in June and July, when a decrease in the tidal range also occurs (Figure 7a). This estuarine suspended sediment mass is mostly composed of the matter transported within the ETM and fluctuates between 4 and 8 Mt according to neap and spring tides during the reference year. This is in agreement with previous studies, which estimated ETM mass variation between 4 to 6 Mt (Allen et al., 1977; Jouanneau, 1979; van Maanen & Sottolichio, 2018).

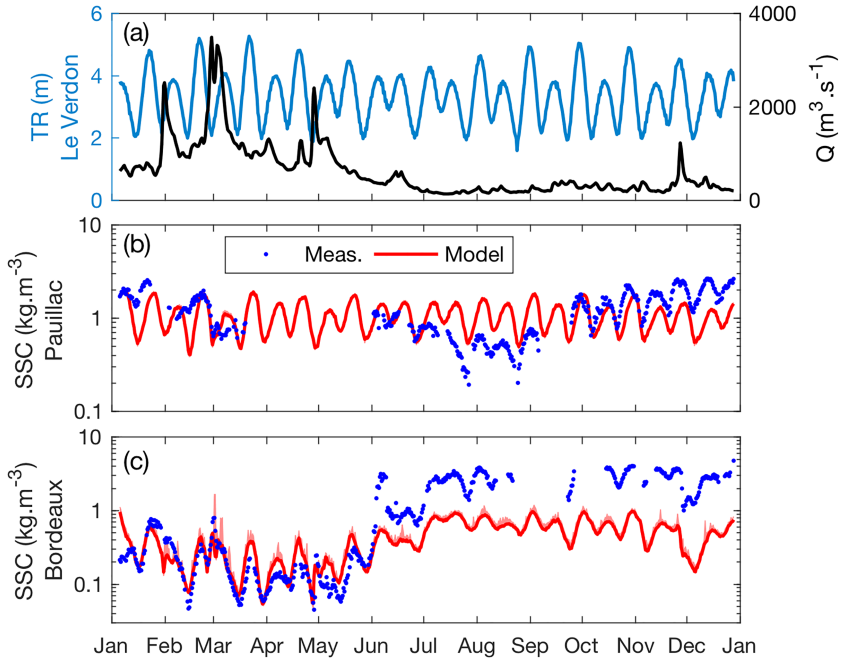

Figure 8. Tide-averaged near-surface (1 m below the surface) SSC dynamics over the year 2015 shown on logarithmic scale. (a) Tidal range at the estuarine mouth (blue, Le Verdon station) and cumulated Garonne and Dordogne river flow Q measured at La Réole and Pessac, respectively (see Figure 1 for exact locations). (b and c) Measured (blue points) and simulated (red line) SSC at (b) Pauillac and (c) Bordeaux (see locations in Figures 1 and 2).

3.2.3. Temporal SSC Dynamics

In this section, the validation of the model is mainly focused on the seasonal and annual dynamics. Tide-averaged (1-hr data averaged between two consecutive peaks of high tides) and near-surface (1 m below the surface) SSCs were measured and simulated throughout the year 2015 at both Pauillac (Figure 8b) and Bordeaux (Figure 8c) stations. The period considered included both high and low river discharge conditions as well as contrasted tidal ranges inducing substantial variations in forcing contributions to sediment dynamics. The SSCs measured at both stations show high sensitivity to the neap-spring cycle, which is well reproduced by the model, with increased resuspension during spring tides due to stronger currents.

The SSC measured at Pauillac tends to increase during high river flow, as the ETM moves downstream, and conversely to decrease in summer when the ETM migrates upstream (Figure 8b). SSC dynamics is reasonably well simulated at this station in terms of the order of magnitude, fortnightly (neap/spring) and seasonal phasing. However, the range of variation of the simulated turbidity is lower compared to measured data and does not show any noticeable seasonal dynamics associated with river flow. Hence, the SSC is overestimated in summer and slightly underestimated at the end of the year. However, these results corroborate previous studies (Jalon-Rojas et al., 2015; van Maanen & Sottolichio, 2018).

The SSC measured at Bordeaux is more significantly modulated by seasonal riverine dynamics than was the case downstream, at Pauillac station. The SSC increases when river flow is low and the ETM upstream (from June to December). Conversely, it decreases when freshwater discharge increases (Figure 8c). The model tends to underestimate the order of magnitude of the SSC during low river flow, when the ETM is located upstream. This can be explained by local resuspensions, which are likely to increase turbidity levels at the measurement station and may not be fully captured by due to the coarse grid cells in this area. However, an increase in simulated concentrations is noticeable from June to December, indicating that the model is able to reproduce the ETM formation and its seasonal migration.

A detailed analysis of SSC at an intratidal time scale is beyond the scope of this study and is already thoroughly described in the literature (Allen et al., 1980; Castaing & Allen, 1981; Sottolichio et al., 2011; van Maanen & Sottolichio, 2018). However, because intratidal dynamics is essential in controlling sediment fluxes, the sensitivity of model results at tidal scale is illustrated in Figure 9, together with the parameterization sensitivity of simulated SSC. Results from test 25 (Figures 9i and 9l) are considered here. At Pauillac station, despite an underestimation of simulated concentrations compared to measurements, the dynamics is well reproduced. Observations reveal an absence of settling at low water slack and large settling at high water slack followed by strong resuspension during peak ebb. At Bordeaux station, however, the measured trend is polluted by the saturation value of the measuring instrument. Besides, the only values "below" the saturation are measured during flood and could have been miscalibrated given the "bell form" of the turbidity sensor calibration law. One hypothesis could be that these measurements actually exceeded the saturation value of the sensor and matched with the wrong domain of the calibration curve. It is thus difficult to conclude about the real dynamics at this location. Therefore, the Pauillac station alone is considered for following comparisons of model outputs and in-situ measurements and for assessing model skills.

The measurements described in this section revealed a strong spatial variability in sediment dynamics, particularly on seasonal time scales (mainly associated with the river flow and the induced ETM location), thus characterizing different environmental conditions along the estuary. This implies that sediment transport empirical parameters can sometimes perform very well locally, while being inadequate and ineffective at other location within the domain. For the purpose of this study, which is to investigate the sediment dynamics behavior associated with equifinal sediment transport parameters, it is assumed that the seasonal sediment dynamic measured at Pauillac is representative of the spatial variability associated with the seasonal ETM migration along the estuary. Sets of sediment transport parameters performing equally well when compared to the reference SSC measurements are first selected to analyze their influence on simulated fluxes between the estuary and the adjacent continental shelf.

3.3. Sensitivity to Sediment Transport Key Parameters

The sensitivity of simulated SSCs to key sediment parameters at the intratidal time scale and as a function of river discharge (averaged by river flow classes) is illustrated in Figure 9. The simulated sediment dynamics are represented for a limited number of model runs, selected to represent the range of simulated SSC

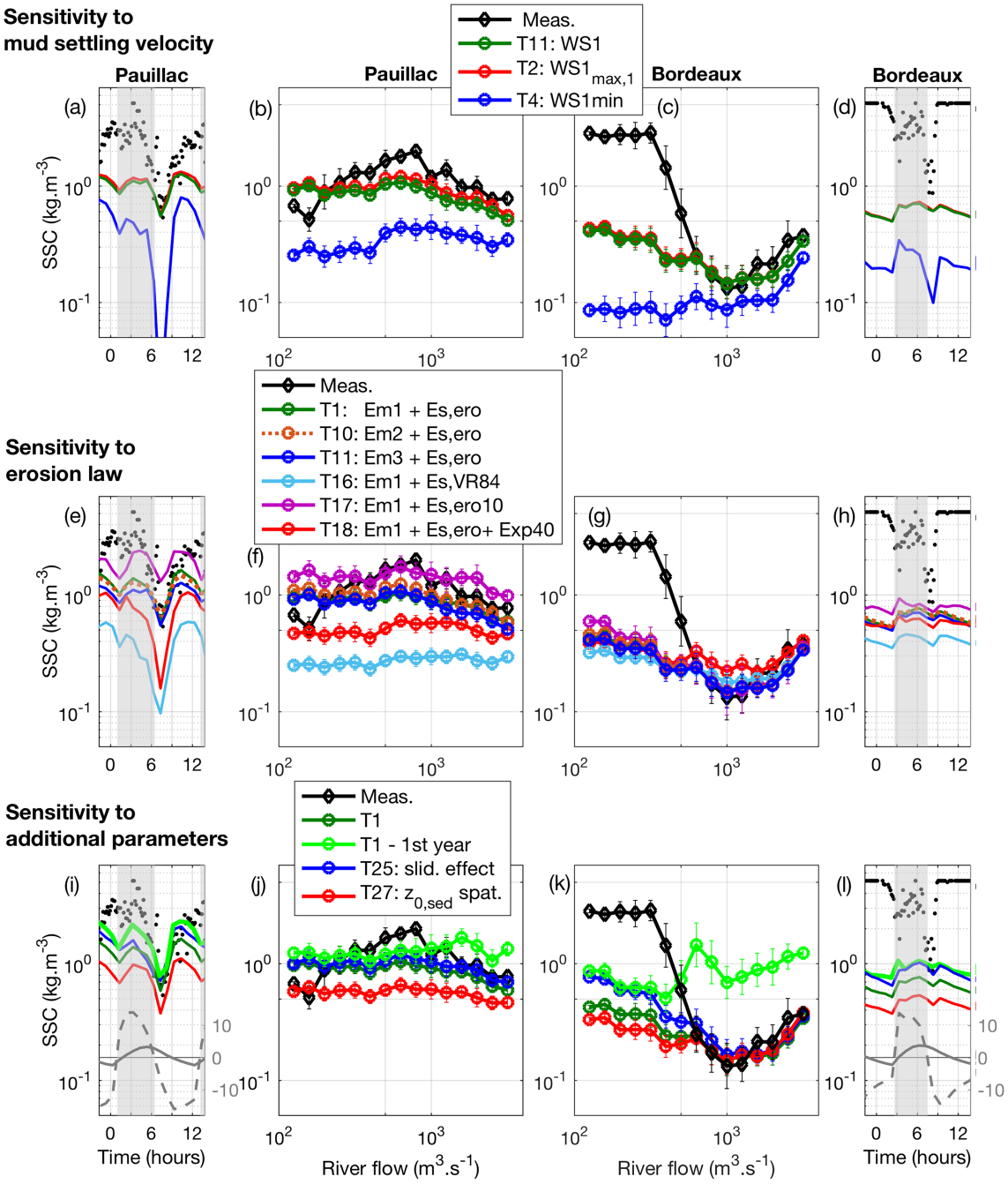

Figure 9. Observed (black) and simulated (colors) comparisons of near-surface SSC at both the intratidal and seasonal time scales associated with changes in (a–d) the mud settling velocity (in $m.s^{-1}$), (e–h) the erosion law, and (i–l) additional parameters described in section 2.3.3. (a, d, e, h, i, and l) Comparisons of SSC time series during one spring tidal cycle and low river flow at (a, e, and i) Pauillac and (d, h, and l) Bordeaux. The gray area represents flood periods (positive tidal current). (i an d l) Gray lines illustrate the local water level in meters (plain lines) and bottom current in $dm.s^{-1}$ (dashed line). (b, c, f, g, j, and k) SSC versus the cumulated Garonne and Dordogne river flow at (b, f, and j) Pauillac and (c, g, and k) Bordeaux. Lines and symbols represent data average associated with river flow ranges (0.1 of log10(Q)), without distinction of tidal conditions. Vertical bars stand for data instantaneous standard deviation (i.e., with no tide-averaging) within the river flow class. Results are plotted on a logarithmic scale. Parameter sets associated with each simulation are listed in Table 1.

behaviors among the tested parameters described in section 2.3 and Appendices C to E. In general, the SSC order of magnitude is well captured by the model at Pauillac station, but the model tends to smooth the seasonal dynamics observed in the measurements (as noticed in Figure 8b). In particular, it is difficult for the model to simulate decreasing SSCs at intermediate and low river flows. At Bordeaux station, however,

the seasonal dynamics are well reproduced, but the model significantly underestimates SSCs for low river flows (e.g., Figure 8c, where the coarse grid cells are unable to capture the local resuspensions measured in-situ).

3.3.1. Sensitivity to Mud Settling Velocity

Changing the contribution of both concentration and turbulence in the computation of mud settling velocity does not significantly impact SSCs at the two stations. Changing the mud settling velocity minimum and maximum limits, however, offers a larger variation range (Figure 9, upper panels). In particular, SSC levels are more sensitive to the minimum settling velocity value ($WS1_{min}$, Test T4) than to the maximum value ($WS1_{max,1}$, Test T2).

At Pauillac station (Figure 9b) for low river flow, SSCs reach 0.3 $kg.m^{-3}$ for a high minimum settling velocity value (0.5 $mm.s^{-1}$, $WS1_{min}$) and 1 $kg.m^{-3}$ for a lower minimum value (0.1 $mm.s^{-1}$, WS1), thus allowing the mud to remain in suspension longer. For higher river flows, the difference is weaker. At a tidal time scale, increasing the minimum value of $w_{s,mud}$ clearly decreases suspended concentrations (Figure 9a). Besides, during high slack tide, mud settling increases with a surface concentration decreasing to zero, while both measurements and other settling velocity calculations indicate concentrations decreasing to 0.5 $kg.m^{-3}$. On the other hand, decreasing the maximum settling velocity value (param. $WS1_{max,1}$) tends to increase SSC levels, particularly during peak flood and ebb, when the suspended concentration increases and the mud settling velocity is likely to reach its maximum value.

At Bordeaux station (Figure 9c), limiting the minimum mud settling velocity to 0.5 $mm.s^{-1}$ instead of 0.1 $mm.s^{-1}$ decreases SSC levels and completely inhibits the ETM migration upstream during period of low river discharge. At first, this appears to contradict the expected upstream migration of the ETM when increasing the mud settling velocity (Brenon & Le Hir, 1999). However, this paradoxical behavior is likely to be induced by an accelerated deposition of fines, which tends to reduce SSC levels in surface waters while modifying the distribution of available sediment and influencing the ETM migration. Similarly to the Pauillac station, it also tends to enhance mud settling during high slack tides. On the other hand, a decrease in the maximum limit (param. $WS1_{max,1}$) tends to increase SSC levels upstream, particularly during low river flow, thus revealing that it contributes to the ETM upstream migration.

At both stations, a similar trend is observed in the contribution of concentration to the computation of $w_{s,mud}$: An increase in $w_{s,mud}$ decreases SSC levels while a decrease tends to increase turbidity (not shown). The tendency is particularly enhanced during low river flow upstream and low to medium river flow at Pauillac, which corresponds to the period at which the ETM is present in these areas. As for the contribution of turbulence, SSC levels are nearly insensitive to its effect on flocculation (not shown).

3.3.2. Sensitivity to Erosion Law

The suspended sediment surface dynamics is compared for different erosion laws, with Test T1 considered as a baseline run (Figure 9 middle panels). In general at Pauillac, SSC dynamics are very sensitive to the erosion behavior, but, as illustrated in Figure 8b, it was difficult for the model to reproduce the ETM migration in the central estuary, where it tends to maintain a somewhat constant and high turbidity independently of the erosion law. At Bordeaux station, on the other hand, changing the erosion dynamics had an effect on the simulated seasonal trend by allowing the ETM to migrate further upstream or by retaining suspended sediment downstream.

In terms of critical shear stress for mud erosion, at Pauillac station, considering a Power 2 dependence on the relative mud concentration increases SSC levels compared to a linear relationship (Formulations Em2 and Em3, respectively). This can be explained by the lower critical shear stress for erosion for nonconsolidated sediment bed in the polynomial equation compared to the linear one ($C_{relmud} < 300$ $kg.m^3$, Figure D1b), the tendency being reversed for consolidated bed. This result reveals that, at Pauillac station, sediment is rapidly eroded and does not significantly consolidate. At Bordeaux stations, however, the difference between the two formulations is not significant, and the simulated turbidity levels are similar. Besides, at both stations, the simulated SSC for a test with a higher critical shear stress for mud erosion (Test T13, not shown) is significantly lower, as a stronger bed shear stress is required to initiate erosion. Unsurprisingly, increasing the mud erosion parameter tends to increase SSC levels at both stations (Test T10), particularly during the period of the ETM presence at both stations. Indeed, during that period, the mud fraction is more likely to be dominant and the prescribed pure mud erosion law to be more often considered.

Multiplying the sand erosion parameter by a factor 10 (Formulation Es,ero10, Test T17; Figure 9 middle panels) increases SSC levels by 65% at Pauillac and by 40% at Bordeaux during low river flow. This result demonstrates that SSC is positively correlated to the sand erosion parameter. When the sediment is noncohesive, the eroded mass is higher for a higher erosion rate parameter. Similarly, the test using the sand erosion formulation of van Rijn (1984) (Es,VR84, Test T16), which reduces $E_{0,\mathrm{sand}}$ (see Figure D1a), results in significantly lower SSCs. However, the magnitude is strongly dependant on the location (e.g., the SSC is reduced by up to 75% at Pauillac and by 25% at Bordeaux during low river flow). Figure 9g shows that simulated SSC at Bordeaux station is sensitive to the prescribed pure sand erosion law both during low and high river flow periods. However, this tendency is reversed during high river flow: considering a lower $E_{0,\mathrm{sand}}$ parameter (Es,VR84, Test T16) tends to increase SSCs.

On the other hand, taking into account an exponential trend between cohesive and noncohesive behaviors (Exp40, Test T18) considerably accelerates the transition from pure sand to pure mud erosion parameters. Therefore, it contributes to decrease both the erosion parameter (Figure D1c) and the exponent n in the Partheniades-Ariathurai formulation (equation 3), while increasing the critical shear stress for erosion for sand/mud mixtures. Figure 9 (middle panels) shows that this test results in up to 47% lower SSC levels at Pauillac and significantly influences simulated seasonal dynamics at Bordeaux. Concentrations are reduced by more than 10% during low river flow, while they increase by up to 55% during intermediate and high river flows. This can be explained by the redistribution of the available stock of sediment, which differs spatially compared to the linear transition trend. Besides, SSC levels are not significantly sensitive to the first critical mud fraction f_{mcr1}, below which a pure sand erosion law is prescribed, particularly with a linear transition (not shown). When an exponential trend is prescribed, the transition is sharper, and reducing the critical mud fraction slightly decreases SSC levels.

3.3.3. Sensitivity to Additional Sediment Transport Parameters

Figures 9j and 9k demonstrate the need for a spin-up period as the seasonal dynamics is not yet in agreement with the measured trends at the two stations. At Bordeaux station in particular, the spin-up simulation does not capture the decreasing SSC for intermediate river flow (~500 $m^3.s^{-1}$). However, despite the model underestimation of turbidity levels for low river flows, sediment dynamics is in better agreement during the second simulated year than during the first one.

The impact of sediment sliding has also been investigated (Test T25). The simulated seasonal dynamics reveals a better agreement with the measured trends when the sliding process is included, particularly in the upper estuary at Bordeaux station. It increases SSC levels for low river flows by up to 80% by limiting the deposition and therefore the trapping of sediment in the upper lateral banks. At Pauillac station, the SSC sensitivity to this effect is less significant, and concentrations are increased by only 15%.

Finally, the influence of the skin bottom roughness was investigated (Tests T26 and T27). Spatializing the skin bottom roughness value with the Nikuradse criteria at each time step tends to significantly decrease its value compared to the baseline test ($z_{0,sed} = 1 \times 10^{-4}$ m). On an annual time scale, it strongly decreases the surface SSC at Pauillac station (Figures 9i and 9j). At Bordeaux, however (Figures 9k and 9l), it tends to decrease SSC levels only for low river flows ($Q < 500$ $m^3.s^{-1}$), thus retaining the ETM downstream during that period.

As mentioned in section 2.3.3, the influence of the number of vertical sigma layers in the water column on sediment dynamics was investigated (not shown). It revealed that increasing the number of layers by a factor of 2 (from 10 to 20 layers) slightly increases SSC levels at the two stations (e.g., by up to 18% for intermediate river flows) but does not change the seasonal trend. Although not shown in this study, an initial fluid mud deposit (1 m thick, 100 $kg.m^{-3}$ concentrated) on the river bed with a mass equal to the expected ETM mass (~4 Mt) was also tested. Interestingly, this had almost no impact on the suspended sediment dynamics after 1 year of spin-up, compared to the baseline run (same initial conditions without the initial fluid mud deposit). This corroborates previous studies, which argued that suspended sediment mass is more related to the estuarine system capacity for stirring sediments rather than to volume of the sediment supply, as long as sufficient sediment is available within the system (Grasso & Le Hir, 2019).

3.4. Skill Assessment

Many statistical techniques are commonly used to assess numerical model performance and particularly sediment transport models (Achete, 2016; Bever & MacWilliams, 2013; Dufois et al., 2018; van Maanen &

Sottolichio, 2018; van Maren & Cronin, 2016). Here, model skills are evaluated following the target diagram methodology described by Jolliff et al. (2009), which is based on commonly used metrics: the model bias normalized by the "reference" standard deviation B^* and the unbiased root-mean-square error normalized by the "reference" standard deviation $RMSE^*$:

$$B^* = \frac{\overline{M} - \overline{D}}{\sigma_D}, \tag{4}$$

$$RMSE^* = \frac{\text{sign}(\sigma_M - \sigma_D)}{\sigma_D} \times \sqrt{\frac{\sum_{n=1}^{N}\left[(M_n - \overline{M}) - (D_n - \overline{D})\right]^2}{N}}, \tag{5}$$

with M and D the modeled and measured data, respectively, $\overline{M}$ and $\overline{D}$ the time-averaged variables and σ_M and σ_D the standard deviation for each field.

As mentioned previously, the Bordeaux station is not taken into account for model skill assessment. In the present study, the "reference" field is thus the MAGEST near-surface SSC measurements at Pauillac station. Therefore, simulated data are considered 1 m below the surface at the corresponding model grid cell. To summarize the statistical information, a target diagram is constructed based on a simple Cartesian coordinate system where $RMSE^*$ is used as the X axis and B^* as the Y axis. $RMSE^*$ was multiplied by the sign of the standard deviation difference: Thus, areas of the diagram where $X < 0$ represent a simulated variability lower than the measured one. Besides, according to the following formulae, the distance between the origin and the statistical points in the diagram is equal to the normalized total standard deviation $RMSE$:

$$RMSE^2 = B^{*2} + RMSE^{*2}. \tag{6}$$

Therefore, the best performing simulation (i.e., with the smallest total $RMSE$) is the one located closest to the origin. These statistical metrics are evaluated by considering both the instantaneous and tide-averaged data. For completeness and for further diagnosis, the B^*, $RMSE^*$, and total $RMSE$ values based on instantaneous data are recorded in Table 1 for each simulation and used in the following section to classify model runs by performance. They were normalized by the reference standard deviation (0.88 at Pauillac and 1.59 at Bordeaux).

The large scatter in target diagrams reveals the sensitivity of the model outputs to the parameterization of sediment transport (Figure 10). The 29 tests performed are represented in Figure 10 (top panels). An unbiased normalized $RMSE^*$ of 1 indicates that the difference between the model and the measurements is as large as the standard deviation of the observations. Therefore, a model with a $RMSE^* > 1$ does not provide any improvement over the time series average and is considered a poor performer. Moreover, a total normalized $RMSE < 1$ indicates that modeled and observed data are positively correlated (see Jolliff et al., 2009, for details). Therefore, a value of 1 provides a good performance marker (gray circles, Figure 10). A normalized total $RMSE$ of 0.85 was selected to represent very good performers (black circles, Figure 10). Target diagrams provide a synthetic picture of model performance while facilitating the comparison of model runs with each other and with observations. The bias B^* refers to the annual mean similarity between model and observations while the $RMSE^*$ indicates a phase and amplitude agreement in the unbiased time series variability. The diagrams were built for the entire simulation period (i.e., 1 year), so that the analyses are focused on annual dynamics. The next step could be to distinguish between seasonal, neap/spring, and tidal time scale metrics to assess model performances at shorter time scales.

Spin-up simulations are more sensitive to sediment parameterization than the second simulated year (red symbols in Figures 10a and 10b). Moreover, the blue symbols (representing the reference year) are generally closer to the origin than the red ones (representing the spin-up year), further supporting the value of analyzing numerical results after a 1-year spin-up. For reference years (blue symbols, Figures 10a and 10b), the scatter distribution is larger for B^* than for $RMSE^*$ (i.e., $RMSE^*$ is less affected than B^* by the various model parameterizations). This means that the simulated SSCs are less underestimated at Pauillac station when the sediment transport model is calibrated.

As mentioned in section 1, the residual sediment transport at the mouth is strongly dependent on the intratidal dynamics (e.g., tidal asymmetry). Therefore, the following analyses and classification of model runs

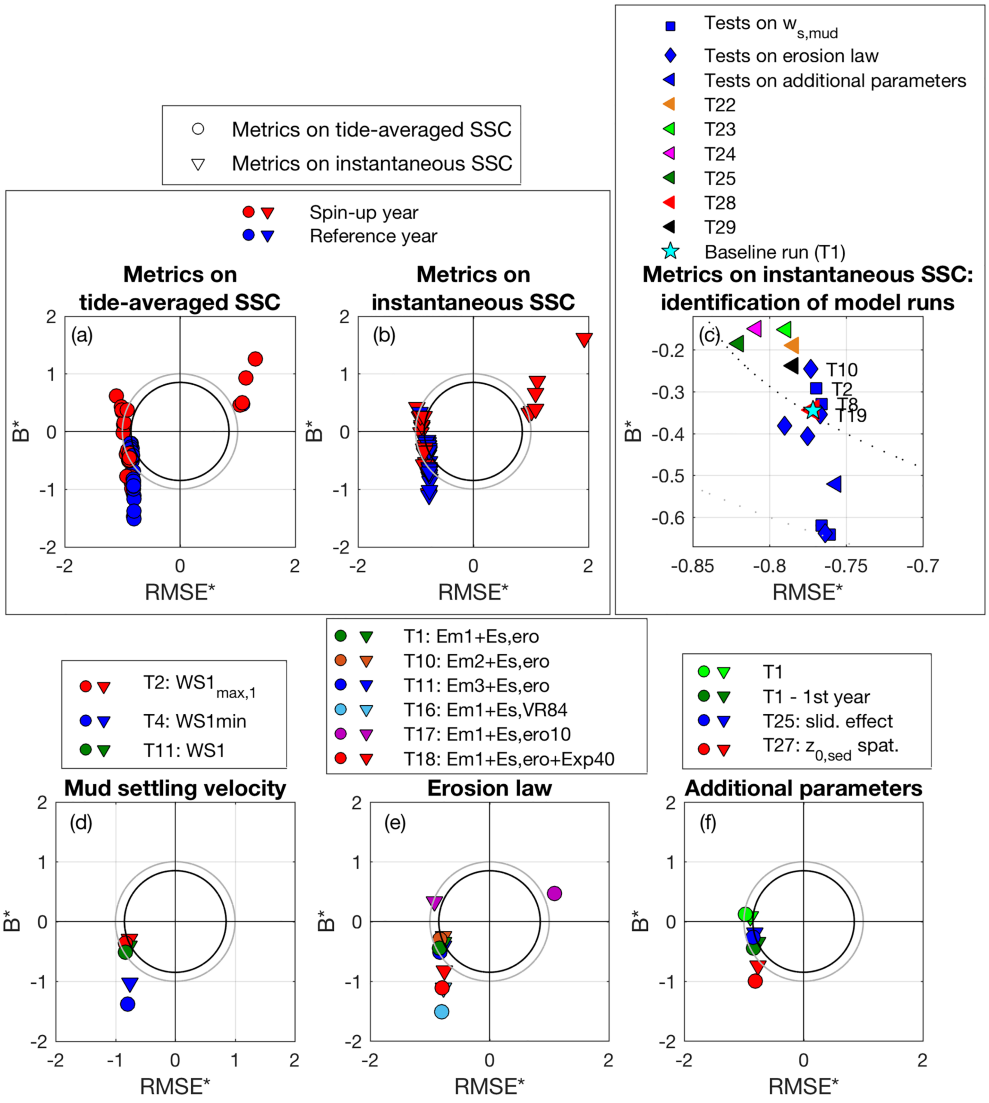

Figure 10. Normalized target diagrams at Pauillac station for (a) tide-averaged (circles) and (b) instantaneous (downward triangles) suspended sediment concentrations for all sensitivity tests described in Table 1, with red markers for the spin-up year and blue markers for the reference year. The thick black and gray lines delineate normalized total RMSE of 0.85 and 1, respectively. (c) A focus on the "very good" performers, with a total normalized RMSE <0.85. Square markers represent tests on mud settling velocity, diamonds represent tests on the erosion law, and leftward triangles illustrate tests on additional parameters. The blue star indicates the baseline run skills. (Bottom) Similar normalized target diagrams for the tests illustrated in Figure 9, showing sensitivity to (d) mud settling velocity limits, (e) erosion law, and (f) additional parameters. Legends are located above each diagram. Circles and triangles represent tide-averaged and instantaneous statistic metrics, respectively.

focused exclusively on their performance relative to instantaneously simulated (reference year) and observed SSCs. A large number of model runs have a total *RMSE* < 1 (18 of the 29 tests, Figure 10c), which can be considered a reasonable score according to Jolliff et al. (2009) and Los and Blaas (2010). Eleven of the 29 tests can be considered as very good performers as their normalized total *RMSE* is lower than 0.85. Most *RMSE** and *B** values are negative, indicating that the model standard deviation is lower than the observed standard deviation and that simulated SSC is smaller than the measurements. However, the T17 test, included in the good performer group with a total *RMSE* of 0.98 (not visible in Figure 10c), has a positive bias indicating an overestimation of the annual mean SSC. In this test, the computed erosion flux in this test has been largely emphasized due to a tenfold increase in the $E_{0,sand}$ (Es, ero10). Very good performers are shown in Figure 10c. The T1 test, which corresponds to the baseline

run, belongs to the very good performers, with the highest total *RMSE* of the group. Taking into account an initially deposited layer of fluid mud (T28) and maximizing f_{mcr1} (T19) have almost no influence on model performances. For the mud settling velocity parameterization, both T2 and T8 tests belong to the very good performers, indicating an improvement of model performances compared to the baseline parameterization. The T10 test, which has a larger $E_{0,\mathrm{mud}}$ than the baseline run (Em2 formulation, see Table D1), also has a normalized total $RMSE < 0.85$. All the tests that took into account the sediment sliding process are also found among the very good performers (Tests T22, T23, T24, and T25, with various percentages). Finally, increasing the number of vertical layers for the simulation appears to improve model performances (e.g., T29 vs. T1).

The gap between instantaneous and tide-averaged metrics for Test T4 dealing with the minimum mud settling velocity is relatively large (Figure 10d). This underlines that changing the minimum mud settling velocity has a significant impact on SSC dynamics at tidal time scales (e.g., by allowing more sediment to settle during slacks for instance). Besides, considering a higher minimum limit (WS1min, T4) considerably deteriorates model skills by increasing bias. On the other hand, lowering the maximum limit of mud settling velocity ($\mathrm{WS1}_{\mathrm{max},1}$, T2) decreases normalized bias, as the simulated SSCs are less underestimated by maintaining sediment in suspension for longer. It should be noted that, for the following analyzes, tests on the mud settling velocity are divided in two groups according to their different erosion laws (tests on the mud settling velocity bounds and tests on the Van Leussen's parameterization; see Table 1). Given these erosion laws, it appears that changing the calibration parameters of mud settling velocity (i.e., c_1 and c_2 param. in equation 1) does not significantly impact model skills (squares on Figure 10c): The largest variability is found in the minimum and maximum values (Figure 10d). Moreover, among all the tested parameterization of mud settling velocity (squares on Figure 10c), $\mathrm{WS1}_{\mathrm{max},1}$ appears to be the best performer (T2, Figures 10c and 10d). For this test, the settling velocity is similar to the baseline run except for SSC values > 0.25 kg.m^{-3} where $w_{s,mud}$ is lower and equal to 1 mm.s^{-1} (Figure C1a).

Changing the erosion law impacts mostly the normalized bias (Figure 10e). Tests using the van Rijn's (1984) formulation (T16) and an exponential transition for sand and mud mixtures (T18) are found to perform poorly (total $RMSE > 1$), because they both considered considerably lower erosion flux, which emphasized the simulated underestimation. For the mud erosion critical shear stress (tide-averaged and instantaneous metrics), choosing a linear or a polynomial formulation within the same range of values does not significantly impact model skills (Em2 vs. Em3 formulations and T10 vs. T11, respectively). As already inferred from Figure 9 (middle panels), this can be explained by the predominance of nonconsolidated sediment, for which both formulations induce similar critical shear stress for erosion. Besides, decreasing the erosion constant for mud ($E_{0,\mathrm{mud}}$) from 0.002 to 0.0003 reduces model skills (Em2 vs. Em1 and T10 vs. T1, respectively). Overall, Figures 10c and 10e show that T10 is the test with the best model skills. Its critical shear stress for mud erosion is similar to the baseline run while $E_{0,\mathrm{mud}}$ is increased (from 3×10^{-4} in the baseline test to 2×10^{-3} in T10).

Figure 10f represents the skills of additional parameters. For the baseline run, despite a lower bias, simulated SSCs after 1-year spin-up are in better agreement with measurements than the first simulated year. Besides, taking into account the sediment sliding process significantly increases model performance (T1 vs. T25). For instantaneous SSCs, the 30% sliding factor performs best (T23, Figure 10c). Finally, the reduction of the bed shear stress obtained by decreasing the bottom roughness strongly reduces the SSC levels and, by reinforcing the underestimation of suspended concentrations, deteriorates model performances as well (at least if the mud shear strength is not modified) (T27 vs. T1, Figure 10f).

As shown on Figures 9 and 10, the results of the SSC simulations are considered satisfactory considering the complexity of the configuration: realistic forcing, multiclass, and multilayer sediment model after 2 years of simulation. Compared to the baseline run, taking into account a higher erosion parameter for mud and the sediment sliding process along a slope limits the underestimation of simulated concentrations. As for the mud settling velocity, the WS4 formulation slightly increases model performance as well. Keeping in mind that the range of parameters tested is not exhaustive and that results could have been different for different parameterizations, simulated SSCs seem more sensitive to the limits of the mud settling velocity than to the parameterization of Van Leussen's law.

4. Sediment Flux Sensitivity to Sediment Parameterization

Numerical modeling of mud and sand transport under realistic conditions and complex environments involves uncertainties associated with the sediment model calibration, which need to be quantified in order to assess model confidence level. In the previous section, the sensitivity of the SSC levels to various sediment transport parameters was presented. The impact of changing these parameters on simulated sediment fluxes at the mouth is discussed below. Fluxes are calculated through the cross section illustrated in Figure 2a (red line), which can be considered as the outer boundary of the estuary. The results are illustrated by time series of cumulative fluxes for total sediment (i.e., the sum of the five classes), as well as for mud and sand classes separately. Positive sediment fluxes are flood directed (i.e., import of sediment into the estuary) and negative values represent export fluxes.

4.1. Mass Flux Dynamics at the Mouth

Both the river seasonal dynamics and neap/spring cycles significantly modulate sediment transport between the estuary and the adjacent continental shelf (Figure 11). By changing the sediment model parameterization, the relative contribution of these forcings to sediment fluxes is more or less pronounced, thus altering the direction and magnitude of the residual sediment mass flux.

In the baseline run (T1, Figure 11 middle vertical panels: green line), residual total sediment fluxes over 1 year are directed up-estuary. Total sediment fluxes are flood directed during the high river flow season due to both estuarine circulation and tidal pumping. This up-estuary mass flux is partly compensated during low river flow by down-estuary fluxes, as sediment is flushed out of the estuary.

The mud and sand dynamics at the mouth are relatively different. However, unlike sands, the residual flux of mud over 1 year is negative, indicating a net export. As described by Castaing and Allen (1981) and revealed by the simulated residual flow (Figure 12a), during high river discharge, the stratification is enhanced, and the baroclinic-induced circulation becomes the main trapping mechanism: The sediment accumulates in the lower estuary where the ETM, and the head of the salt intrusion is located. However, during spring tides, large amounts of sediments are injected in the upper part of the water column and are likely to be exported to the shelf by the surface seaward density-induced surface outflow (Figure 12c). This phenomenon is illustrated on the cumulated fluxes in Figure 11b by decreasing steps, particularly at the end of March during periods of high river flow and strong spring tides combined. Such a behavior is particularly evident for mud fluxes, as mud is more likely to reach the upper part of the water column than sands. It is easily readable for T17 (pink line, Figures 11b and 11e) because the erosion flux is multiplied by 10. In contrast, during neap tides, the reinforced stratification strengthens the up-estuary baroclinic circulation, driving strong import of sediment into the estuary (Figure 12d).

On the other hand, during low river flow, Castaing and Allen (1981) measured a net sediment flux directed seaward during spring tides. Such seaward fluxes are limited to the upper part of the water column during mean and neap tides, with near-bed residual fluxes directed landward. In Figure 12b, the simulated residual currents also reveal that the stratification is weaker during the dry season, leading to a reduced density circulation. Vertical profiles of velocity and SSCs tend to be more homogeneous, and, as sediments reach the near-surface area during spring tides, they are more likely to be exported seaward (Figure 11 middle vertical panels). Again, this is readable from the baseline run and emphasized for T17 (pink line, Figure 11 middle vertical panels). During mean and neap tides, however, sediments, and particularly sands and gravels, are transported up-estuary with near-bottom currents. This leads to a residual import of sand and gravel into the estuary over the year and a substantially accretive lower estuary.

4.2. Sensitivity to Sediment Transport Key Parameters

The sensitivity of the simulated sediment flux to the model parameterization is illustrated in Figure 11 for a selection of tests representing the flux variability observed across all tests. This sensitivity is also illustrated in Figure 13 (upper panels), where the mean annual residual fluxes at the mouth are illustrated, regardless of the model run performance previously described. In addition, annual absolute fluxes are computed as the cumulative sum of the absolute value of instantaneous fluxes (Figure 13, lower panels). It mostly provides knowledge about the intensity of the sediment mass dynamics at the mouth, regardless of the direction, and reveals that small residual transport values can result from strong absolute dynamics. Subsequent "compensated" (i.e., residual) fluxes associated with tidal, neap/spring, and seasonal time scales may be

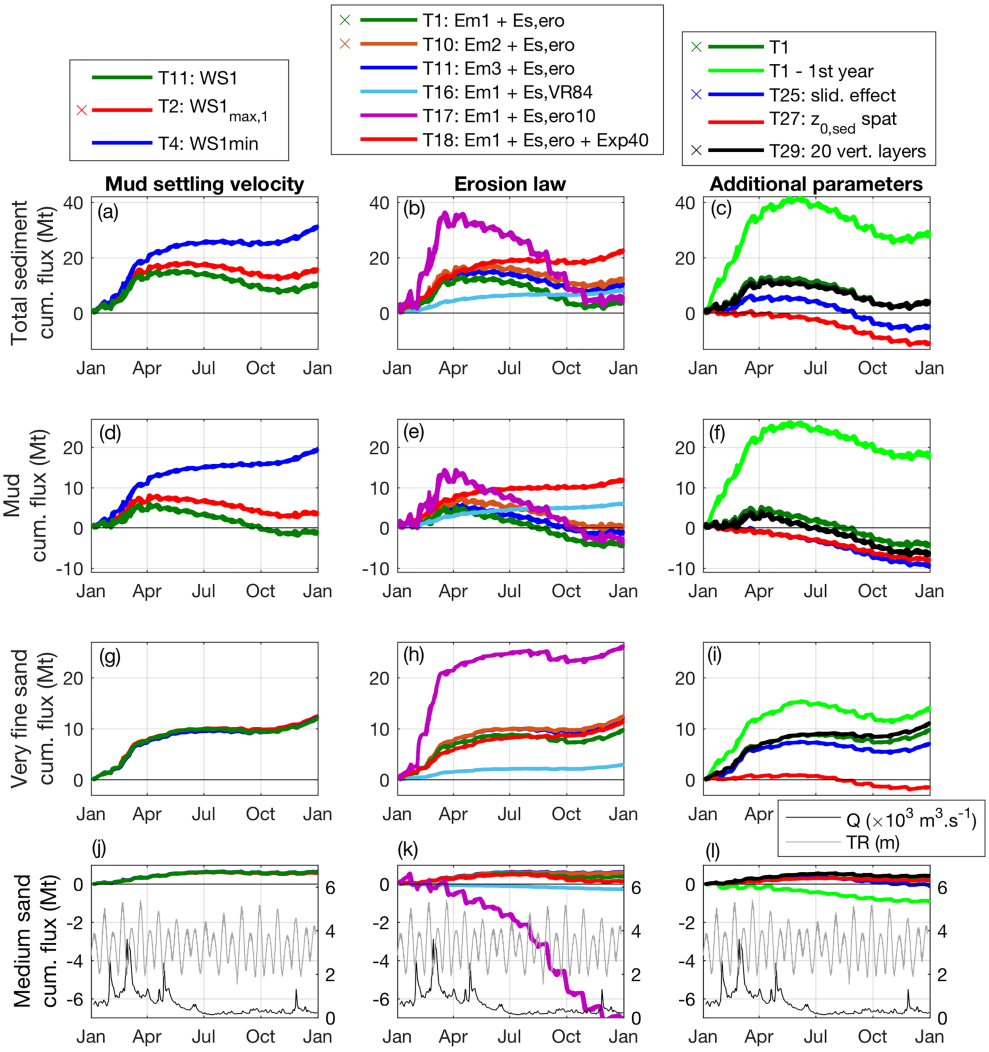

Figure 11. Time series of cumulative fluxes of (a–c) total sediment, (d–f) mud, (g–i) very fine sand (d = 100 μm) and (j–l) medium sand (d = 400 μm) associated with different parameterization including (a, d, g, and j) mud settling velocity, (b, e, h, and k) erosion law, and (c, f, i, and l) other sediment transport parameters. Fluxes are calculated at the estuarine mouth across the red-line section illustrated in Figure 2a: Positive fluxes indicate sediment import into the estuary, and negative fluxes indicate sediment export toward the continental shelf. Very good performers are identified in the legend by ×. (j–l: right axis) Time series of the Garonne and Dordogne river flow (black line, $\times 10^3$ m^3.s^{-1}) and tidal range at the mouth (gray line).

highly energetic and drive large mass exchanges between the estuary and the continental shelf. For instance, the annual residual flux for mud is lower than the one for very fine sand (see Figure 13b); however, its annual absolute value is drastically larger (see Figure 13e), illustrating the contrasted sediment exchanges at the estuary mouth. Figure 13 also highlights that finer particles fluxes are the most dynamic and are responsible for most of the total sediment fluxes.

4.2.1. Mud Settling Velocity

Similarly to Figure 9 (top panels) for SSC, the simulated sediment fluxes are more sensitive to changes in $w_{s,min}$ than $w_{s,max}$. Increasing $w_{s,min}$ leads to an increase in mud import into the estuary because the mud settles more quickly and is more likely to be transported near the bottom where the residual current velocities are directed up-estuary (Figure 12). It also limits the variations associated with river flow and the net export of sediment during low river flow. In contrast, a lower maximum mud settling velocity (Test T2) also reduces the net export of particles during low river flow, ending up in a flood-directed residual mud mass flux after 1 year, given the other assigned parameters.

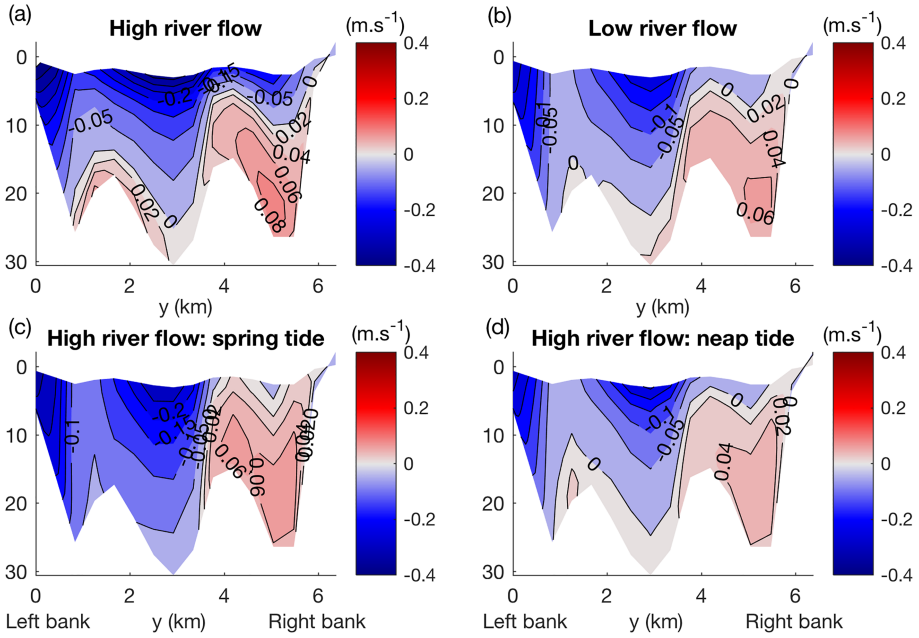

Figure 12. Residual velocities at the estuarine mouth through the red-line cross section illustrated in Figure 2a (positive up-estuary, vertical reference: mean sea level). Average over a neap/spring cycle during periods of (a) high river flow and (b) low river flow. Average during high river flow during (c) spring tide and (d) neap tide periods of 7 days.

The sensitivity of the simulated sediment flux to the mud settling velocity is illustrated in Figure 13 (left panels), where they are divided by tests on $w_{s,mud}$ limits and on Van Leussen's law parameterization (dark and light gray, respectively). Changing the mud settling velocity mostly impacts the simulated mud fluxes but does not significantly impact the dynamics of noncohesive classes (see brackets in Figure 13a, ±5.0 Mt for mud and ±0.8 Mt for very fine sand). Considering that the prescribed erosion laws are different between the two groups, no further conclusion can be drawn from the mean values of the annual residual fluxes, which are significantly different. However, the standard deviations, illustrated by brackets in Figure 13, show that the simulated residual fluxes are more sensitive to the minimum and maximum settling velocity value than to the parameterization of Van Leussen's equation.

4.2.2. Erosion Law

Increasing the mud erosion parameter (T10) tends to enhance the total sediment up-estuary residual flux, as more sediments are resuspended and transported with the baroclinic up-estuary circulation. This reveals that modifying the mud erosion law strongly affects total sediment fluxes by modifying both mud and sand fluxes at the mouth (Figures 11e, 11h, and 11k). This is similar with the pure sand erosion law: decreasing the pure sand erosion flux, by changing the transitional trend or the sand erosion parameter (T16 and T18), or increasing it (T17) significantly impacts both mud and sand mass fluxes. Besides, decreasing the erosion flux also limits the influence of seasonal and neap/spring signals on sediment flux dynamics while reducing the erosion flux.

Although the tendencies could have been different with other baseline parameters (e.g., a different settling velocity parameterization) or tested values, the residual mud fluxes are directed up-estuary in tests with limited erosion fluxes and offshore in the other tests (Figure 11e). Lower erosion flux is likely to change the spatial redistribution of the available sediments. Both situations could lead to fewer particles reaching the upper part of the water column and, then, to a reduction of the seaward surface flux when the density circulation is well developed. There is a residual import of very fine sand for all tests on erosion law (Figure 11h). Increasing the sand erosion flux drastically increases the import of very fine sand up-estuary during periods of high river flow, resulting from the reinforced up-estuary baroclinic circulation. For the coarser sand dynamics, the residual mass flux for a stronger sand erosion flux is directed seaward. This is mostly driven by strong export during spring tides (Figure 11k), and particularly during low river flow, as already inferred from measurements by Castaing and Allen (1981). The different behaviors between the very fine and

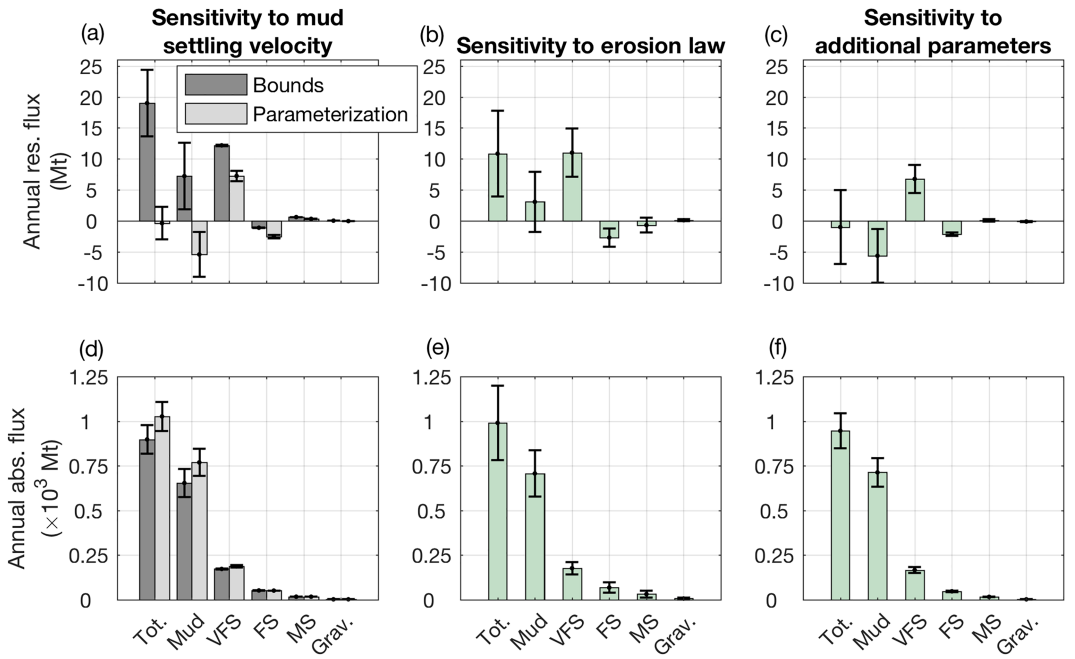

Figure 13. (Top) Annual residual fluxes and (bottom) annual absolute fluxes of total sediment (Tot.), mud, very fine sand (VFS), fine sand (FS), medium sand (MS), and gravel (Grav.) through the mouth for (a and d) tests on mud settling velocity limits (dark gray) and Van Leussen's law parameterization (light gray), (b and e) tests on erosion law, and (c and f) tests on additional parameters. Bars indicate mean values for the corresponding sediment class and test category, and brackets represent the associated standard deviations.

medium sands, resulting in opposite residual flux directions for a larger sand erosion flux, highlight the complex interactions between tidal current asymmetries and critical shear stress for erosion, which differs for each sediment class. Besides, the Figure 12 shows strong horizontal velocity gradients, which could play a significant role in sediment mass fluxes, as the suspended sediment nature is possibly different between the left and the right bank due to the presence of both the Saintonge (near the right bank) and the main navigation channels. However, it is beyond the scope of this study to further describe the lateral behavior of the sediment fluxes (McSweeney et al., 2016; Ross et al., 2017; Ross et al., 2019).

Changing the erosion law mostly impacts residual mud and very fine sand fluxes (±4.8 and ±3.9 Mt, respectively; Figure 13b), which fluxes are the most dynamic. It has a small impact on the simulated coarser sands fluxes (±1.5 Mt for fine sand and ±1.2 Mt for medium sand). Both residual and absolute mud fluxes are very sensitive to the prescribed erosion law, thus revealing the sensitivity of mud dynamics to the mud class parameterization as well as the sand dynamics. It also highlights that, given the variability in the simulated fluxes at the mouth, it is crucial to calibrate the erosion law thoroughly.

4.2.3. Additional Sediment Transport Parameters

Sediment fluxes are significantly larger in the first year of simulation, as the model redistributes the sediment classes over the domain (Figure 11 right panels, T1 and T1-1st year). The Gironde Estuary mouth is a highly energetic area (tidal current velocities >1.5 $m.s^{-1}$) where particles are eroded and, during high river flows, transported into the estuary where they are trapped on intertidal banks. The simulated dynamics is similar for total sediment and noncohesive classes during the two simulated years, but sediment fluxes are weaker after 1 year of spin-up. Mud fluxes are flood directed during high river flow and ebb directed during the dry season. However, after 1 year of spin-up, the residual net transport is reversed compared to the first year. There is a residual export of mud at the end of the reference year, while mud was significantly imported into the estuary during the spin-up year. This is explained by the adjustment of the model to a mud-dominated environment in the estuary and a sand-dominated environment on the continental shelf.

Adding the sediment sliding process (T1 vs. T25) reverses the up-estuary transport of mud during high river flow. Sediments trapped on the lateral banks slide into the channel where they are resuspended and transported out of the estuary with the net seaward estuarine surface circulation.

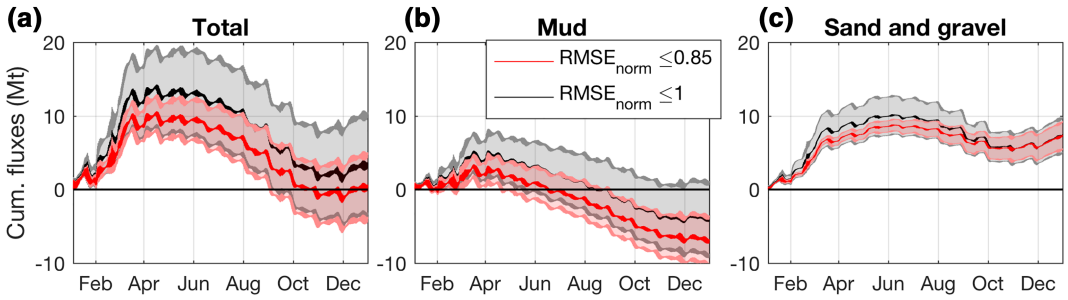

Figure 14. Cumulative mean fluxes of (a) total sediment, (b) mud, and (c) sand and gravel classes and their associated standard deviations for the "very good performers" (red) and for the "good performers" (black), characterized by a normalized RMSE ≤0.6 and ≤1, respectively. The total vertical shaded area represents the computed standard deviations, centered on the mean value.

The net mud transport at the mouth behaves differently compared to the baseline run for a spatialized skin roughness length varying between 3×10^{-6} and 5×10^{-5} mm, while it was set at 1×10^{-4} for other simulations (T1 vs. T27). As expected and already inferred from Figures 9j and 9k, reducing the skin roughness length strongly decreases SSC values and considerably impacts the fluxes at the mouth. The mud flux is directed offshore throughout the year. Similarly, fluxes of very fine sand are significantly different from the baseline run with residual fluxes directed offshore. A lower $z_{0,sed}$ results in lower bed shear stresses and erosion flux and weaker suspended sediment dynamics. Thus, both tidal pumping, induced by asymmetrical currents along the estuary, and the gravitational-induced transport are reduced.

Finally, the vertical stratification is better reproduced and the induced gravitational circulation more pronounced when the number of vertical layers is increased. Consequently, the residual export of mud to the shelf and the import of noncohesive classes into the estuary are enhanced (Figure 11 right panels).

4.3. Quantification of Sediment Flux Uncertainties

A thorough quantification of model uncertainties associated with simulated fluxes is difficult to achieve as no observations are available for comparisons. In the previous section, the sensitivity of simulated sediment fluxes to various sediment transport parameters was discussed. The finest particle classes, and especially the mud class, are the most sensitive to changes in sediment transport parameters (up to ±130 Mt standard deviation for absolute fluxes considering changes in the erosion law, Figure 13e). The large discrepancies identified in this study, therefore, highlight the need for quantifying model prediction uncertainties.

Based on the SSC model performances (instantaneous values) described in section 3.3.4, model runs are classified as "very good performers" (normalized $RMSE \leq 0.85$) or "good performers" (normalized $RMSE \leq 1$). Tests identified as "poor performers" (i.e., with a normalized $RMSE > 1$; 11 of the 29 tests) were set apart and not discussed further. It is important to note that the group of "good performers" (18 tests) also includes the "very good performers" (11 tests identified in Figure 10c). The resulting uncertainties associated with model performance are illustrated in Figure 14 using time series of cumulative mean fluxes and their associated standard deviations. Results for total sediment, mud, and "sand and gravel" fluxes, the latter including the four noncohesive classes (three sands and one gravel), are represented separately.

The computed uncertainty related to sediment transport model parameterization can be evaluated using the standard deviation associated with equifinal parameter sets. Uncertainties for very well and well-performing simulations are shown in Figure 14 and summarized below:

$$\begin{cases} \text{Total sediment flux} = 0.4 \pm 4.4 \text{ Mt for } RMSE \leq 0.85 \text{ and } 3.4 \pm 6.8 \text{ Mt for } RMSE \leq 1 \\ \text{Mud flux} = -7.0 \pm 3.3 \text{ Mt for } RMSE \leq 0.85 \text{ and } -4.0 \pm 4.9 \text{ Mt for } RMSE \leq 1 \\ \text{Sand and gravel flux} = 7.3 \pm 1.9 \text{ Mt for } RMSE \leq 0.85 \text{ and } 7.4 \pm 2.4 \text{ Mt for } RMSE \leq 1 \end{cases}.$$

The mean total sediment residual fluxes for both groups of tests are significantly different (0.4 and 3.4 Mt for very good performers and good performers, respectively), as well as the associated standard deviations (4.4 and 6.8 Mt, respectively; Figure 14a), with a larger dispersion of residual fluxes for good performers. The same behavior is observed for mud residual fluxes (4.9 Mt for "good performers" vs. 3.3 Mt for the

very good ones; Figure 14b), as well as for "sand and gravel" fluxes (2.4 Mt vs. 1.9 Mt, respectively; Figure 14c). This means that smaller SSC simulation errors also decrease the dispersion of residual sediment fluxes.

Mud export at the mouth (-7 ± 3.3 Mt) is large compared to the fluvial mud import within the estuary (around -1.5 Mt), meaning that there is no direct balance between estuarine mud export and fluvial mud import. Therefore, some parts of the estuary act as sediment sources.

4.4. Discussion

Calibration is a necessary step when using complex numerical modeling, in order to ensure confidence in model results. In particular, model predictive skills and ability to reproduce real system behavior needs to be assessed in order to ensure the model's ability to provide additional understanding of system behavior. Numerous parameterization tests are usually necessary to achieve this process and to select the best parameter set. Based on these performed runs, this study goes beyond the classical calibration and validation phase and provides additional information on system and model behavior.

Model results revealed the importance of running a spin-up period before the analysis. Because the sediment initial distribution is set as uniform, the model needs a period of adjustment in order to reach a (quasi-)equilibrium state through the redistribution of the sediment coverage. The duration of the spin-up period depends on the system under study and the model parameterization. In this study, a spin-up period of 1 year was considered for the sediment transport model, as the available computational facilities allowed it (about 24 hr computation is needed for 1-year simulation). Moreover, the comparison of sediment fluxes after 1- and 2-year spin-up demonstrated that 1 year of spin-up is sufficient to reach a near dynamic equilibrium state (see Figure G1 and details in Appendix G).

While the calibration process is a necessary step and helps to identify the most performant parameter sets, the sensitivity analysis revealed that a better reproduction of surface SSCs contributes to reduce uncertainties on simulated fluxes at the mouth and to lower uncertainties on the prediction of both mud and "sand and gravel" fluxes. Interestingly, reducing the error on SSC simulations tends to emphasize the difference between mean residual mud and "sand and gravel" fluxes (-7.0 and 7.3 Mt, respectively for very good performers vs. -4.0 and 7.4 Mt for good performers; Figure 14), while the mean residual fluxes of the "sand and gravel" class is stable for good and very good performers (7.4 vs. 7.3 Mt, respectively). However, quantifying the uncertainty associated with very good performers revealed a dispersion around the mean value of about 93% for mud and 51% for sand and gravel classes together. This suggests that the calibration/validation approach is incomplete: Using surface SSC measurements to calibrate a numerical sediment transport model mostly focuses on improving the simulated mud dynamics, as noncohesive classes have a higher settling velocity and are unlikely to reach the upper part of the water column. The first step toward improvement could be to use bottom SSCs or sand transport rate measurements to evaluate the model's performances in order to catch bottom suspended dynamics and vertical gradients. Besides, the equifinal parameter sets characterized in this study are mainly due to a lack of validation data, which are not representative of the complexity of the simulated physical processes. Equifinality could be mitigating during calibration by using laboratory measurements of mud settling velocity or critical shear stress.

Analyzing the sediment dynamics at the mouth, as revealed by the simulated fluxes, highlights a residual export of mud toward the shelf and an import of sand into the estuary, which identified the lower estuary as an accretion area. Similar dynamics have been assessed in the past (Mallet et al., 2000). Residual currents were in agreement with the simulated behavior, with a flood-dominated lower part of the water column and an ebb-dominated upper part. Besides, the presence of shell fragments in the sedimentary facies of the lower estuary, upstream of the outer estuarine boundary, also corroborates a substantial import of marine sand into the estuary in this area (Kapsimalis et al., 2004). Only a qualitative validation of the sediment budget is possible due to the large uncertainties associated with estimating in-situ fluxes. Castaing and Jouanneau (1987) estimated mud fluxes at the shelf around about 1.5 Mt.year^{-1}, which is lower than the mean residual fluxes simulated with the best model runs in the present study (7.0 ± 3.3 Mt.year^{-1}). However, this estimation is questionable and must be considered with care, because it was obtained by spatially and temporally extrapolating a fixed measurement over one tidal cycle. A similar model tendency to

overestimate the exported mud mass between the Gironde Estuary and the shelf has already been experienced in previous studies (van Maanen & Sottolichio, 2018).

A further detailed analysis of the model sensitivity to depositional setting may prove meaningful, as it appears from this study that deposition rates may be too large compared to horizontal transport. Lower deposition fluxes may result in higher SSC levels for higher settling velocities as horizontal transport may become dominant. Besides, residence times are not discussed further in this work, because it is beyond the scope of this sensitivity analysis and uncertainty quantification. Yet they would be crucial to understand better the fate of contaminants in a fluvial-estuarine-shelf system. For instance, residence times could be investigated by tracing sediment particles within the sediment model and analyzing their dynamics.

Model results also revealed a strong seasonal variability of the sediment fluxes at the mouth. For mean residual fluxes of very good performers (Figure 14a), about 10 Mt of sediments are imported into the estuary over the 3 months of high river flow, while a total of 6 months of low river flow are necessary to flush this sediment out of the estuary. Another interesting feature highlighted in this study is the larger up-estuary transport through the mouth during high river flow. It seems to contradict the expected effect of high river flow (shifting the ETM seaward and flushing more sediments offshore), although the same behavior was simulated by Schulz et al. (2018) for the Seine Estuary. While more fine sediment is exported at the surface in the turbid plume, the up-estuary transport dominates due to a stronger stratification during high river flow, which has the effect of strengthening the estuarine baroclinic circulation. Little was known of this behavior in the system under study so far, and it would be interesting to investigate it in more detail using field measurements.

5. Conclusions

Based on a three-dimensional realistic process-based hydrodynamic and sediment dynamic model of the Gironde Estuary (France), the influence of sediment transport key parameters on sediment transfers between a macrotidal estuary and the adjacent continental shelf were investigated. Sensitivity tests were carried out to quantify model uncertainties on mud and sand fluxes along the land-sea continuum.

Comparing model outputs with observations revealed that the model accurately reproduces water levels, currents, and salinity fields on semidiurnal to annual time scales. High-frequency SSC measurements in the estuary were compared with sediment transport model outputs and used to study mud and sand suspended dynamics on seasonal to annual time scales. It was found that the model reproduced the observed sediment dynamics reasonably well, despite an underestimation of suspended concentrations during low river flow in the ETM area.

To investigate the influence of model parameterization on simulated sediment dynamics, a sensitivity analysis was conducted taking into account changes in key sediment parameters such as mud settling velocity, erosion law, and skin roughness length. For this purpose, a total of 29 simulations of 2 years each were performed. Based on model skills to reproduce SSCs and following an equifinality approach, these numerical tests were classified into two groups of very good and good performers to further study their influence on simulated sediment fluxes at the estuary mouth.

Both estuarine circulation and tidal pumping induce residual up-estuary fluxes of sediment at the mouth, compensated by significant seaward fluxes during spring tides and low river flow, in agreement with previous studies. However, the relative contribution of neap/spring and river flow forcing to sediment transfers is more or less emphasized depending on the sediment model parameterization. First, it was found that performing a 1-year spin-up simulation before the analysis is of major importance to ensure the relevance of the sediment model results in terms of both suspended dynamics and fluxes at the mouth. As expected with a sediment transport model accounting for mud and sand mixtures, the mud class is the most dynamic in terms of exchanges with the open ocean, further assessing the importance of quantifying these fluxes as well as residence times, in case of contamination by pollutants.

Considering the parameter sets of the very good performer group, the quantification of the uncertainties associated with annual residual fluxes revealed a dispersion of about 93% for mud and 51% for sand and gravel classes together. A first step to improve the simulation of sediment fluxes is to use bottom measurements to compare with modeled SSCs. In doing so, the model's ability to reproduce suspended sand

concentrations, as well as SSC vertical gradients and changes in bed composition, would be included in the validation process. Moreover, using data measured at the exact same location as the cross section used in this study would be ideal for assessing model performances. A further key point is the thorough quantification of sediment fluxes along the estuary cross sections. Such field measurements are difficult to collect but would be very useful to further constraint the model parameterization and assess its ability to reproduce realistic sediment exchanges in estuaries.

These uncertainties are depending on the tested parameter sets and their range of variation. The "real" uncertainties are likely to be larger, as some processes characterizing sediment models were not investigated (e.g., the deposition flux formulations). However, as most of the estuarine sediment transport processes and patterns occur in the study area and were implemented in the model, the results of the present work, including sediment dynamic responses and uncertainties associated with the key sediment transport parameters, can be reliably extrapolated to other estuarine systems with similar characteristics.

Appendix A: Hydrodynamic Model Description

The computed bottom orbital wave velocity U_w is used to calculate the wave-induced bed shear stress as $\tau_w = \frac{1}{2}\rho f_w U_w^2$ (Jonsson, 1967) with $\rho = 1{,}025$ kg.m^{-3} the water density and $f_w = 0.015$ the wave friction parameter. The current-induced bed shear stress is expressed as $\tau_c = \rho u_*^2$ where u_* is determined from the turbulent boundary layer theory:

$$u(z1) = \frac{u_*}{\kappa}\ln\left(\frac{z1}{z_{0,sed}}\right),$$

with $u(z1)$ the current velocity at mid-elevation of the bottom cell and $z_{0,sed}$ the skin bottom roughness length.

The total bed skin shear stress is expressed as a combination of the current- and wave-induced bed shear stresses (Soulsby, 1997) as follows:

$$\tau = \left[(\tau_{cw} + \tau_w|\cos\ \Phi|)^2 + (\tau_w\ \sin\ \Phi)^2\right]^{\frac{1}{2}},$$

with Φ the angle between the current and the orbital wave velocities and τ_{cw} the current-induced bed shear stress influenced by waves expressed as

$$\tau_{cw} = \tau_c\left[1 + 1.2\left(\frac{\tau_w}{\tau_c + \tau_w}\right)^{3.2}\right].$$

Appendix B: Erosion Law Parameterization

The sediment behaves as noncohesive sediment below a first critical mud fraction (f_{mcr1}), and the prescribed erosion regime follows the formulation of pure sand erosion. The critical shear stress for pure sand erosion $\tau_{ce,sand}$ is determined following the Shields criteria formulated by Soulsby (1997). The sand erosion rate formulation $E_{0,\mathrm{sand}}$ was derived from erodibility measurements (Le Hir et al., 2008) and reads

$$E_{0,sand} = \tau_{ce,sand}^{n_{sand}}\min\left(0.27, 10^3\left\langle d_{50,sand}\right\rangle - 0.01\right), \tag{B1}$$

with $d_{50,sand}$ the weighted mean diameter of sand classes in the surficial layer and $n_{sand} = 1.6$. This formulation is later referred as "Erodimetre formulation" or "Es,ero."

Above a second critical mud fraction f_{mcr2} (typically 0.7; Le Hir et al., 2011), a cohesive erosion behavior is defined. In this case, the typical n_{mud} exponent is set to 1, thus prescribing a linear erosion flux formulation (Grasso et al., 2018; Le Hir et al., 2011; Mengual et al., 2017; Schulz et al., 2018; van Maanen & Sottolichio, 2018), and the mud erosion rate $E_{0,\mathrm{mud}}$ is set at a constant value (see section 2.3.2.2 and Appendix D for details on prescribed value). The critical shear stress for pure mud is considered varying with the consolidation state of the sand-mud mixture that is assumed to be represented by the relative mud concentration C_{relmud} (Le Hir et al., 2011; Waeles et al., 2008). A classical power law is adopted:

$$\tau_{ce,mud} = x_1 C_{relmud}^{x_2}, \quad \text{(B2)}$$

where x_1 and x_2 are calibration parameters.

For a transitional content of mud ($f_{mcr1} > f_m > f_{mcr2}$), an interpolation method is prescribed between noncohesive and cohesive behaviors. Based on literature and experimental works (Le Hir et al., 2008; Panagiotopoulos et al., 1997; van Ledden et al., 2004), the erosion-related parameters are interpolated from the two previously described erosion laws (i.e., pure sand or pure mud) following a transition trend that has to be specified (see section 2.3.2.3 and Appendix D).

Appendix C: Mud Settling Velocity Sensitivity Tests

Minimum and maximum baseline values (test T1) are set at $w_{s,min} = 1 \times 10^{-4}$ m.s^{-1}, $w_{s,max} = 2 \times 10^{-3}$ m.s^{-1}, and the effect of salinity is considered for all tests (not considered by Grasso et al., 2018).

The sensitivity to the weight of the suspended mud concentration C_{mud} in the $w_{s,mud}$ calculation is first studied by changing c_1 and c_2 parameters in equation 1 (Figure C1a and Table C1). Its contribution is alternatively reduced (e.g., formulation WS3 where the c_2 exponent is set to 1 instead of 0.79 in WS1 parameter set) and increased (e.g., the WS2 formulation, where c_1 is two times WS1) compared to the baseline parameters. By drastically reducing c_1 while increasing both c_2 and the maximum $w_{s,mud}$ value, the resulting mud settling velocity is significantly lowered with the WS5 parameterization (derived from Thorn & Parsons, 1980, calibration parameters, without accounting for the hindered settling regime), compared to the baseline parameterization.

The minimum and maximum bounds of w_s are also varied (Table C1 and Figure C1a, green plain and dashed lines): Compared to WS1, the minimum value is multiplied by 5 (Test WS1$_{min}$), which contributes to speed up the mud settling, and the maximum value is either divided by 2 (Test WS1$_{max,1}$) or multiplied by 1.3 based on the Thorn and Parsons (1980) observed maximum value (test WS1$_{max,2}$).

Moreover, the effect of turbulence to the mud settling velocity calculation is studied. The a and b parameters (equation 1) associated with shear rate G contribution are either set at 0.3 and 0.18, respectively, based on calibration values of Grasso et al. (2018), or set to 0 in order to neglect turbulence effect on flocculation (Tests WS5 and WS6; Figure C1b and Table C1).

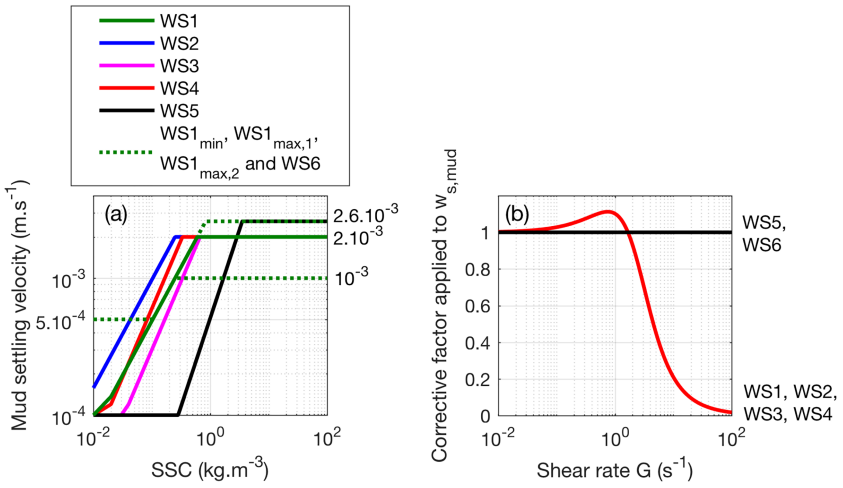

Figure C1. (a) Mud settling velocity as a function of the mud concentration: Plain lines represent variations of c_1 and c_2 parameters in equation 1, and dashed green lines illustrate variations of minimum and maximum values ($w_{s,min}$ and $w_{s,max}$, respectively). (b) Corrective factor applied to the mud settling velocity associated with the shear rate.

Table C1
Tested Parameters of Equation 1 Associated With the Mud Settling Velocity

		c_1	c_2	a	b	$w_{s,min}$ (m s^{-1})	$w_{s,max}$ (m s^{-1})
WS1	Grasso et al. (2018)	0.003	0.79	0.3	0.18	1×10^{-4}	2×10^{-3}
WS1$_{min}$		0.003	0.79	0.3	0.18	**5×10^{-4}**	2×10^{-3}
WS1$_{max,1}$		0.003	0.79	0.3	0.18	1×10^{-4}	**1×10^{-3}**
WS1$_{max,2}$		0.003	0.79	0.3	0.18	1×10^{-4}	**2.6×10^{-3}**
WS2		**0.006**	0.79	0.3	0.18	1×10^{-4}	2×10^{-3}
WS3		0.003	**1**	0.3	0.18	1×10^{-4}	2×10^{-3}
WS4		**0.006**	**1**	0.3	0.18	1×10^{-4}	2×10^{-3}
Ws5	Thorn and Parsons (1980)	**0.000513**	**1.29**	**0**	**0**	1×10^{-4}	**2.6×10^{-3}**
WS6		0.003	0.79	**0**	**0**	1×10^{-4}	**2.6×10^{-3}**

Note. Terms in bold are those that differ from the baseline paremeterization.

Appendix D: Erosion Law Sensitivity Tests

D.1. Noncohesive Sediment Behavior

Regarding the sand erosion flux parameter, the formulation from van Rijn (1984) denoted as "Es,VR84," also based on flume experiments, is tested (Figure D1a). It reads

$$E_{0,sand} = 0.000005\,\rho_s \left(\frac{(s-1)^{0.6} g^{0.6} d_{50,sand}^{0.8}}{\nu^{0.2}} \right), \tag{D1}$$

$s = \rho_s/\rho$ the relative density, ρ_s the sediment density (kg.m^{-3}), g the gravity acceleration (m.s^{-2}), and ν the fluid kinematic viscosity (m^2.s^{-1}). The coefficient in equation D1 is different from the one originally prescribed by van Rijn (1984) as the reference height considered for the erosion, and deposition flux computation in our model is different from the one he used. It should also be noted that the flume experiments conducted by van Rijn (1984) where performed with low flow conditions in the range 0.5–1.5 m.s^{-1}. A modified sediment pickup function has recently been formulated by van Rijn et al. (2019) to extend the validity scope of the formulation to higher velocities (1.5 to 6 m.s^{-1}) and to a wider range of sand diameters, but it has not yet been implemented and tested in this study.

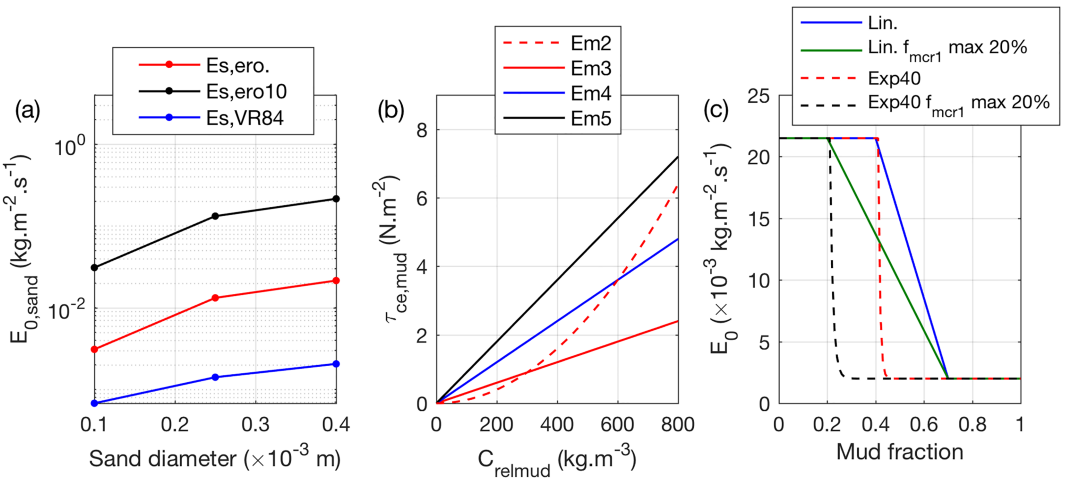

Figure D1. (a) Different formulations of the erodibility coefficient for noncohesive behavior $E_{0,sand}$ as a function of the sand diameters. (b) Critical shear stress for cohesive sediment erosion as a function of the relative mud concentration: variations of x_1 and x_2 values. (c) Variations of the erodibility parameter E_0 as a function of the surficial mud content for different transition trends for a given sand size of 400 μm.

Table D1
Tested Parameters of Equation B2 and the Associated $E_{0,mud}$ for Cohesive Sediment Erosion

		x_1	x_2	$E_{0,\mathrm{mud}}$ (kg·m^{-2}·s^{-1})
Em1	Grasso et al. (2018)	0.00001	2	0.0003
Em2		0.00001	2	**0.002**
Em3		**0.003**	**1**	**0.002**
Em4		**0.006**	**1**	**0.002**
Em5		**0.009**	**1**	**0.002**
Em6		**0.003**	**1**	**0.0002**
Em7		**0.006**	**1**	**0.0002**

Note. Terms in bold are those that differ from the baseline paremeterization.

D.2. Cohesive Sediment Behavior

The critical shear stress for mud erosion ($\tau_{ce,mud}$) is strongly related to the sediment consolidation state (equation B2). Variations in $\tau_{ce,mud}$ modify both the initiation of motion threshold and the quantity of suspensions. Therefore, it is likely that the induced effect on SSC and on sediment fluxes is not proportional to the changes in the $\tau_{ce,mud}$ value. The baseline parameterization for pure mud erosion law is based on the calibration by Grasso et al. (2018) for the Seine Estuary (Em1, Table D1). Depending on the x_2 parameter (equation B2), a linear formulation was tested, associated with several values of x_1 parameter, as illustrated in Figure D1b and readable in Table D1.

D.3. Transitional Behavior

For a transitional content of mud ($f_{mcr1} > f_m > f_{mcr2}$), two types of transition were tested: (i) a linear transition where the erosion-related parameters are linearly interpolated from the sand and mud erosion parameters (used as the baseline parameterization) and (ii) an exponential transition (Mengual et al., 2017). Both transition trends were applied to the three erosion-related parameters (i.e., τ_{ce}, E_0 and n) as a function of mud content (Figure D1c). A coefficient C_{exp} has to be defined to adjust the sharpness of the exponential transition and, as proposed by Mengual et al. (2017), a value of 40 was chosen in this study (referred to as Exp40, Test T18, Table 1).

The beginning of transitional behavior was also tested. Le Hir et al. (2011) observed that this critical mud fraction (f_{mcr1}) linearly increases with the mean sand diameter and suggested, followed by Mengual et al. (2017), to express it as

$$f_{mcr1} = \alpha_0 d_{50,sand}.$$

The parameter α_0 was set to 1,000 m^{-1} for the baseline parameterization leading to f_{mcr1} varying in the range 0.1–0.4 considering the sand classes prescribed in this work (see section 2.2.2). In order to study the impact of this critical parameter on sediment fluxes, a simulation was performed with f_{mcr1} maximized at 0.2 (denoted as "f_{mcr1} *max* 20%") (Figure D1c and Test T19 in Table 1). The second critical mud fraction f_{mcr2} (above which a pure cohesive behavior is considered) is fixed at 0.7 based on Le Hir et al. (2011), and its influence on sediment fluxes has not been investigated. It should still be noted that for an exponential transition formulation, the f_{mcr2} parameter does not really act as a critical threshold anymore, given the abrupt transition (Figure D1c).

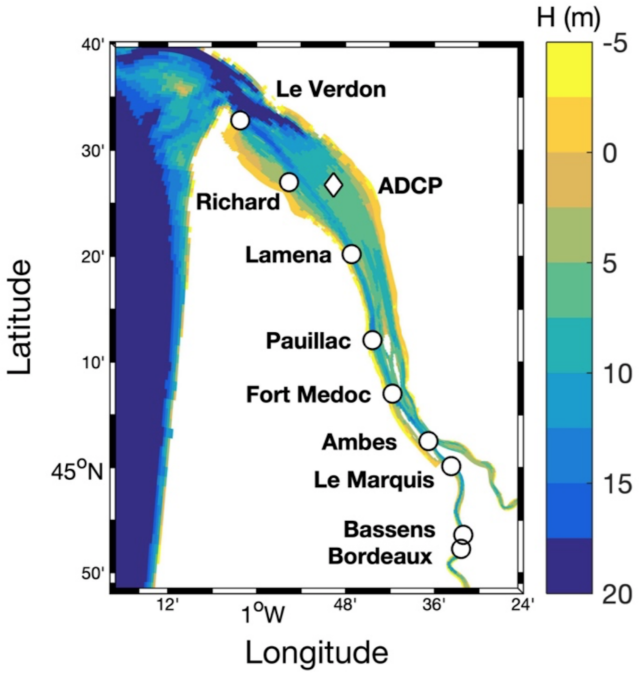

Figure F1. A zoom on the estuary and its bathymetry (mean sea level chart datum). The white circles locate the measurement points for water level, and the white diamond represents the ADCP location.

Appendix E: Sensitivity Tests for Additional Parameters

E.1. Sediment Sliding Process

In MARS3D, the sediment sliding process can be simulated by assigning a part of the deposition flux from one cell to the neighboring one based on the slope between the two cells. The amount of fresh deposit transported to a deeper adjacent cell depends on a prescribed percentage of the slope. The steeper the slope, the bigger the part of the deposition flux affected to the lower cell. In order to emphasize (or reduce) the contribution of this process, the prescribed percentage can be enhanced (or respectively lowered). This process enables to reintroduce suspended sediment in the deepest areas of the system (e.g., channels) when trapped on shallow areas (e.g., tidal flats). The baseline parameterization does not account for this

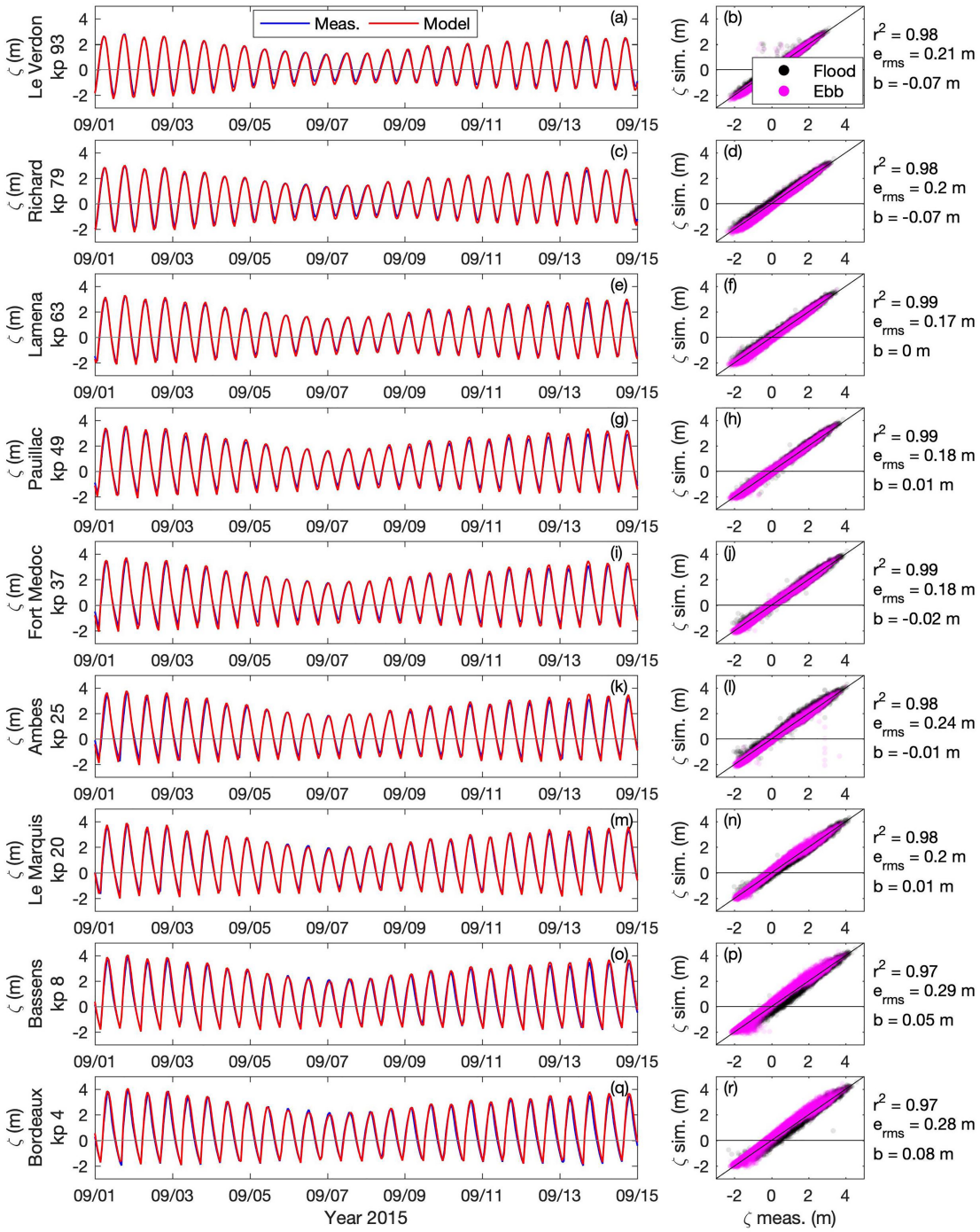

Figure F2. Water level at every station illustrated by white circles in Figure F1 from top to bottom, respectively, from downstream to upstream. (left) Time series of measurements (blue) and simulations (red) from 1 to 15 September 2015. (right) Simulated elevations against in-situ data during flood (black dots) and ebb (pink dots) with the corresponding correlation coefficient r^2, the root-mean-square error e_{rms} and the bias *b*. *kp* is the kilometric point associated with every station along the Gironde Estuary, with $kp = 0$ in Bordeaux.

process. However, for the purpose of following sensitivity analysis, several values of sliding parameter have been tested: 15%, 30%, 50%, and 100% (Table 1).

E.2. Skin Roughness in the Bed Shear Stress Computation

Following Nikuradse formulation $z_{0,\text{sed}} = \frac{k_s}{30}$ with $k_s = 3d_{50}$, the Nikuradse roughness coefficient, a skin bottom roughness constant value of 1×10^{-4} m corresponds to a mean grain size of 1 mm. Two other

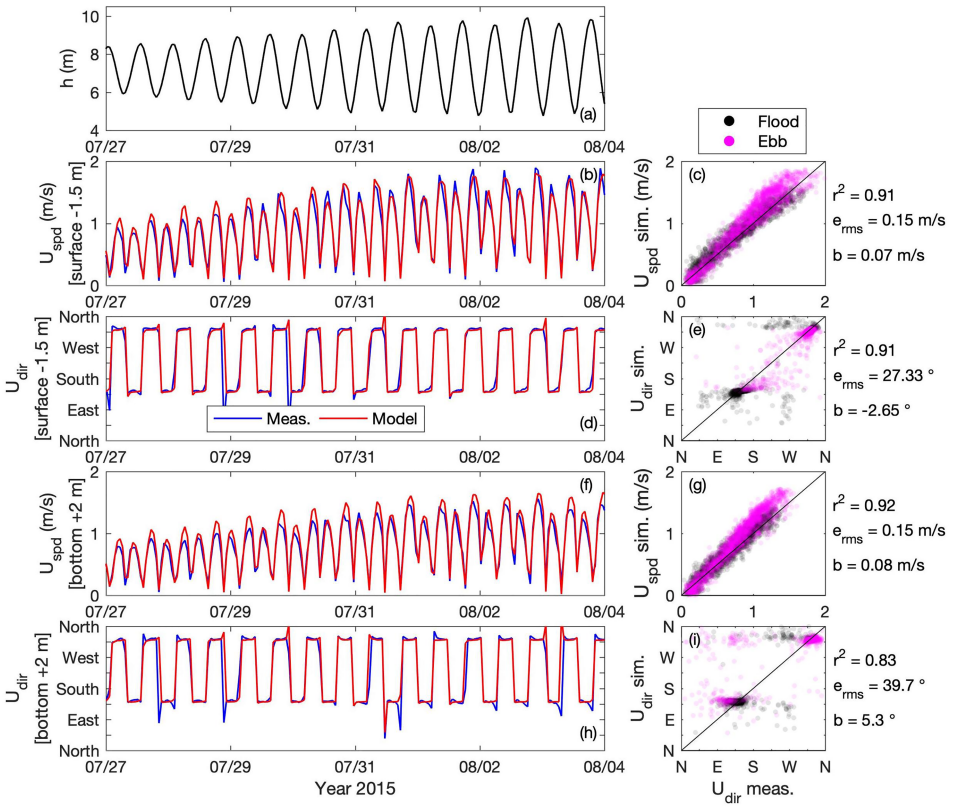

Figure F3. (a) Water level h simulated at the ADCP mooring location (see Figure F1). (b and c) Current intensity and (d and e) direction 1.5 m under the surface. (f and g) Current intensity and (h and i) direction 2 m above the bed. (b, d, f, and h) Time series of measurements (blue) and model outputs (red) from 27 July to 4 August 2015. (c, e, g, and i) Simulated against in-situ data during flood (black dots) and ebb (pink dots) with the squared correlation coefficient r^2, the root-mean-square error e_{rms}, and the bias b.

simulations were tested: a constant value of $z_{0,sed} = 5 \times 10^{-5}$ m, characterizing a mean grain size of 500 μm (test T26) and a spatially and time varying $z_{0,sed}$, based on the Nikuradse formulation and on the local mean grain size at each time step and in each cells (Test T27).

E.3. Cross-Sensitivity Tests

As illustrated in Figure D1c, both the exponential transitional trend and the maximum value of f_{mcr1} were varied simultaneously in the T20 experiment, following recommendation from Mengual et al. (2017). Moreover, similarly to the approach proposed by van Maren and Cronin (2016) consisting in combining several parameter variations likely to have partly compensating effects, another test was performed (T21, Table 1) where both the sand erosion constant was increased ("Es,ero10") and the transitional behavior was sharpened ("Exp40"). As illustrated in Figure D1c, considering an exponential transition trend leads to a strongly reduced erosion flux. Applying a large $E_{0,\mathrm{sand}}$ (multiplied by 10) may compensate this effect on the suspended sediment dynamics and generate an equifinal parameter set.

Appendix F: Additional Validation of the Hydrodynamic Model

The simulated water levels were calibrated by adjusting the form roughness length parameter used in the bottom friction calculation (different from the above-mentioned skin bottom roughness length considered for sediment erosion). It is controlled by the bedform characteristics deduced from the local grain size, which is determined by the maximum current velocity. The computed form roughness was reduced in the upper or central estuary depending on the river flow to represent the reduction of friction by ETM induced fluid mud. The simulated water levels were also better reproduced by taking into account the meteorological surges at

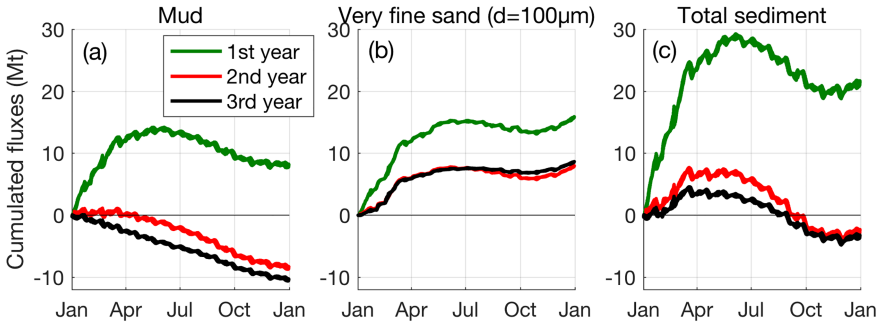

Figure G1. Time series of cumulative fluxes of (a) mud, (b) very fine sand (d = 100 µm), and (c) total sediment for three consecutive realistic year 2015 (first year: green; second year: red; and third year: black line).

the sea boundary. Thus, following this methodology, the model revealed a good accuracy in reproducing water levels along the estuary with a minimum root-mean-square error (e_{rms}) of 17 cm at Lamena station (Figure F2; see Figure F1 for location).

The current vertical structure (i.e., surface and bottom velocities) has also been compared and presented similar skills as the depth-averaged current: $e_{rms} \leq 0.15$ m.s^{-1} and bias $b \leq 0.08$ cm.s^{-1} (Figure F3).

Appendix G: Sediment Fluxes Sensitivity to Spin-up Years

A third realistic year 2015 was performed in order to ensure that considering a 1-year spin-up prior to the year of analysis is sufficient (Figure G1). Unlike the first and the second simulated fluxes at the estuarine mouth, which are very different, the second and third year fluxes are very similar. This confirms that the model is near dynamic equilibrium after a 1 year spin-up.

Acknowledgments
This work was done as part of the AMORAD project and received a state fund managed by the Agence Nationale de la Recherche (ANR) under the program Investissements d'avenir (AMORAD-ANR-11-RSNR-0002). We warmly thank Florent Lyard and Damien Alain (UMR LEGOS, Toulouse, France) for the development of the curvilinear mesh tool POCVIP and their technical support for configuring the curvilinear grid used in this study. Finally, we also would like to thank Sabine Schmidt (UMR EPOC, Bordeaux, France) for providing the MAGEST data (data are available at www.magest.u-bordeaux1.fr). Model data are available online at (ftp://ftp.ifremer.fr//ifremer/dataref/curviseine/curvigironde).

References

Achete, F. M. (2016). *Multiple scales of suspendend sediment dynamics in a complex geometry estuary*. The Netherlands: IHE Delft Institute for Water Education.

Aksoy, H., & Kavvas, M. L. (2005). A review of hillslope and watershed scale erosion and sediment transport models. *Catena*, *64*(2–3), 247–271. https://doi.org/10.1016/j.catena.2005.08.008

Allen, G. P. (1971). Déplacements saisonniers de la lentille de "crème de vase" dans l'estuaire de la Gironde. *Comptes Rendus de l'Académie des Sciences*, *273*(Series D, 2429–2431.

Allen, G. P., Salomon, J. C., Bassoullet, P., Dupenhoat, Y., & Degrandpre, C. (1980). Effects of tides on mixing and suspended sediment transport in macro-tidal estuaries. *Sedimentary Geology*, *26*(1–3), 69–90. https://doi.org/10.1016/0037-0738(80)90006-8

Allen, G. P., Sauzay, G., & Castaing, P. (1977). Transport and deposition of suspended sediment in the Gironde Estuary, France. In *Estuarine processes* (pp. 63–81). New York: Elsevier.

Beven, K. (1993). Prophecy, reality and uncertainty in distributed hydrological modeling. *Advances in Water Resources*, *16*(1), 41–51. https://doi.org/10.1016/0309-1708(93)90028-E

Bever, A. J., & MacWilliams, M. L. (2013). Simulating sediment transport processes in San Pablo Bay using coupled hydrodynamic, wave, and sediment transport models. *Marine Geology*, *345*, 235–253. https://doi.org/10.1016/j.margeo.2013.06.012

Bi, Q. L., & Toorman, E. A. (2015). Mixed-sediment transport modelling in Scheldt Estuary with a physics-based bottom friction law. *Ocean Dynamics*, *65*(4), 555–587. https://doi.org/10.1007/s10236-015-0816-z

Brenon, I., & Le Hir, P. (1999). Modelling the turbidity maximum in the Seine Estuary (France): Identification of formation processes. *Estuarine, Coastal and Shelf Science*, *49*(4), 525–544. https://doi.org/10.1006/ecss.1999.0514

Burchard, H., & Baumert, H. (1998). The formation of estuarine turbidity maxima due to density effects in the salt wedge. A hydrodynamic process study. *Journal of Physical Oceanography*, *28*(2), 309–321. https://doi.org/10.1175/1520-0485(1998)028<0309:TFOETM>2.0.CO;2

Burchard, H., Schuttelaars, H. M., & Ralston, D. K. (2018). Sediment trapping in estuaries. *Annual Review of Marine Science*, *10*(1), 371–395. https://doi.org/10.1146/annurev-marine-010816-060535

Castaing, P., & Allen, G. P. (1981). Mechanisms controlling seaward escape of suspended sediment from the Gironde—A macrotidal estuary in France. *Marine Geology*, *40*(1–2), 101–118. https://doi.org/10.1016/0025-3227(81)90045-1

Castaing, P., & Jouanneau, J. (1987). Les apports sédimentaires actuels d'origine continentale aux océans. *Bulletin de l'Institut de Géologie du Bassin d'Aquitaine*, *41*, 53.

Chapman, P. M., & Wang, F. (2001). Assessing sediment contamination in estuaries. *Environmental Toxicology and Chemistry*, *20*(1), 3–22.

Coynel, A. (2005). Erosion mécanique des sols et transferts géochimiques dans le bassin Adour-GaronneI. Bordeaux 1.

Demerliac, M. (1974). Calcul du niveau moyen journalier. *Annales hydrographiques du SHOM*, *549*, 49–57.

Dijkstra, Y. M., Schuttelaars, H. M., Schramkowski, G. P., & Brouwer, R. L. (2019). Modeling the transition to high sediment concentrations as a response to channel deepening in the Ems River Estuary. *Journal of Geophysical Research: Oceans*, *124*, 1578–1594. https://doi.org/10.1029/2018JC014367

Doxaran, D., Froidefond, J. M., Castaing, P., & Babin, M. (2009). Dynamics of the turbidity maximum zone in a macrotidal estuary (the Gironde, France): Observations from field and MODIS satellite data. *Estuarine, Coastal and Shelf Science*, *81*(3), 321–332. https://doi.org/10.1016/j.ecss.2008.11.013

Dufois, F., Lowe, R. J., Rayson, M. D., & Branson, P. M. (2018). A numerical study of tropical cyclone-induced sediment dynamics on the Australian north west shelf. *Journal of Geophysical Research: Oceans*, *123*, 5113–5133. https://doi.org/10.1029/2018JC013939

Dyer, K. R. (1989). Sediment processes in estuaries—Future-research requirements. *Journal of Geophysical Research*, *94*(C10), 14,327–14,339. https://doi.org/10.1029/JC094iC10p14327

Festa, J. F., & Hansen, D. V. (1978). Turbidity maxima in partially mixed estuaries—2-Dimensional numerical-model. *Estuarine and Coastal Marine Science*, *7*(4), 347–359. https://doi.org/10.1016/0302-3524(78)90087-7

French, J. R. (2010). Critical perspectives on the evaluation and optimization of complex numerical models of estuary hydrodynamics and sediment dynamics. *Earth Surface Processes and Landforms*, *35*(2), 174. https://doi.org/10.1002/esp.1899

Fuentes-Cid, A., Etcheber, H., Schmidt, S., Abril, G., De-Oliveira, E., Lepage, M., & Sottolichio, A. (2014). Dynamics of coarse particulate matter in the turbidity maximum zone of the Gironde Estuary. *Comptes Rendus Geoscience*, *346*(1–2), 28–36. https://doi.org/10.1016/j.crte.2014.03.001

Geyer, W. R. (1993). The importance of suppression of turbulence by stratification on the estuarine turbidity maximum. *Estuaries*, *16*(1), 113. https://doi.org/10.2307/1352769

Grasso, F., & Le Hir, P. (2019). Influence of morphological changes on suspended sediment dynamics in a macrotidal estuary: Diachronic analysis in the Seine Estuary (France) from 1960 to 2010. *Ocean Dynamics*, *69*(1), 83–100. https://doi.org/10.1007/s10236-018-1233-x

Grasso, F., Le Hir, P., & Bassoullet, P. (2015). Numerical modelling of mixed-sediment consolidation. *Ocean Dynamics*, *65*(4), 607–616. https://doi.org/10.1007/s10236-015-0818-x

Grasso, F., Verney, R., Le Hir, P., Thouvenin, B., Schulz, E., Kervella, Y., et al. (2018). Suspended sediment dynamics in the macrotidal Seine Estuary (France): 1. Numerical modeling of turbidity maximum dynamics. *Journal of Geophysical Research: Oceans*, *123*, 558–577. https://doi.org/10.1002/2017JC013185

Huijts, K. M. H., Schuttelaars, H. M., de Swart, H. E., & Valle-Levinson, A. (2006). Lateral entrapment of sediment in tidal estuaries: An idealized model study. *Journal of Geophysical Research*, *111*, C12016. https://doi.org/10.1029/2006JC003615

Jalon-Rojas, I., Schmidt, S., & Sottolichio, A. (2015). Turbidity in the fluvial Gironde Estuary (southwest France) based on 10-year continuous monitoring: Sensitivity to hydrological conditions. *Hydrology and Earth System Sciences*, *19*(6), 2805–2819. https://doi.org/10.5194/hess-19-2805-2015

Jolliff, J. K., Kindle, J. C., Shulman, I., Penta, B., Friedrichs, M. A. M., Helber, R., & Arnone, R. A. (2009). Summary diagrams for coupled hydrodynamic-ecosystem model skill assessment. *Journal of Marine Systems*, *76*(1–2), 64–82. https://doi.org/10.1016/j.jmarsys.2008.05.014

Jonsson, I. G. (1967). Wave boundary layers and friction factors. In *Coastal engineering 1966* (pp. 127–148). New York: American Society of Civil Engineers.

Jouanneau, J. M. (1979). Evaluation du volume et de la masse des matieres en suspension dans le systeme bouchon vaseuxcreme de vase de la Gironde. *Bulletin Institut de Géologie du Bassin d'Aquitaine*, *25*(1979, 111–120.

Jouanneau, J. M., Weber, O., Cremer, M., & Castaing, P. (1999). Fine-grained sediment budget on the continental margin of the Bay of Biscay. *Deep-Sea Research Part Ii-Topical Studies in Oceanography*, *46*(10), 2205–2220. https://doi.org/10.1016/S0967-0645(99)00060-0

Kapsimalis, V., Masse, L., & Tastet, J. P. (2004). Tidal impact on modern sedimentary facies in the Gironde Estuary, southwestern France. *Journal of Coastal Research*, *41*, 1–11.

Krone, R. B. (1962). Flume studies of transport of sediment in estrarial shoaling processes. *Final Report, Hydr. Engr. and Samitary Engr. Res. Lab., Univ. of California*.

Lajaunie-Salla, K., Wild-Allen, K., Sottolichio, A., Thouvenin, B., Litrico, X., & Abril, G. (2017). Impact of urban effluents on summer hypoxia in the highly turbid Gironde Estuary, applying a 3D model coupling hydrodynamics, sediment transport and biogeochemical processes. *Journal of Marine Systems*, *174*, 89–105. https://doi.org/10.1016/j.jmarsys.2017.05.009

Lazure, P., & Dumas, F. (2008). An external-internal mode coupling for a 3D hydrodynamical model for applications at regional scale (MARS). *Advances in Water Resources*, *31*(2), 233–250. https://doi.org/10.1016/j.advwatres.2007.06.010

Le Floch, J.-F. (1961). Propagation de la marée dans l'estuaire de la Seine et en Seine-Maritime: Propositions données par la Faculté, Université de Paris.

Le Hir, P., Cann, P., Waeles, B., Jestin, H., & Bassoullet, P. (2008). Erodibility of natural sediments: Experiments on sand/mud mixtures from laboratory and field erosion tests. *Proceedings in Marine Science*, *9*, 137–153. https://doi.org/10.1016/S1568-2692(08)80013-7

Le Hir, P., Cayocca, F., & Waeles, B. (2011). Dynamics of sand and mud mixtures: A multiprocess-based modelling strategy. *Continental Shelf Research*, *31*(10), S135–S149. https://doi.org/10.1016/j.csr.2010.12.009

Lesueur, P., Tastet, J. P., & Marambat, L. (1996). Shelf mud fields formation within historical times: Examples from offshore the Gironde Estuary, France. *Continental Shelf Research*, *16*(14), 1849–1870. https://doi.org/10.1016/0278-4343(96)00013-1

Lesueur, P., Tastet, J. P., & Weber, O. (2002). Origin and morphosedimentary evolution of fine-grained modern continental shelf deposits: The Gironde mud fields (Bay of Biscay, France). *Sedimentology*, *49*(6), 1299–1320. https://doi.org/10.1046/j.1365-3091.2002.00498.x

Los, F. J., & Blaas, M. (2010). Complexity, accuracy and practical applicability of different biogeochemical model versions. *Journal of Marine Systems*, *81*(1–2), 44–74. https://doi.org/10.1016/j.jmarsys.2009.12.011

Mallet, C., Howa, H., Garlan, T., Sottolichio, A., Le Hir, P., & Michel, D. (2000). Utilisation of numerical and statistical techniques to describe sedimentary circulation patterns in the mouth of the Gironde Estuary. *Comptes Rendus De L Academie Des Sciences Serie Ii Fascicule a-Sciences De La Terre Et Des Planetes*, *331*(7), 491–497. https://doi.org/10.1016/S1251-8050(00)01437-3

McSweeney, J. M., Chant, R. J., & Sommerfield, C. K. (2016). Lateral variability of sediment transport in the Delaware Estuary. *Journal of Geophysical Research: Oceans*, *121*, 725–744. https://doi.org/10.1002/2015JC010974

McSweeney, J. M., Chant, R. J., Wilkin, J. L., & Sommerfield, C. K. (2017). Suspended-sediment impacts on light-limited productivity in the Delaware Estuary. *Estuaries and Coasts*, *40*(4), 977–993. https://doi.org/10.1007/s12237-016-0200-3

Mengual, B., Le Hir, P., Cayocca, F., & Garlan, T. (2017). Modelling fine sediment dynamics: Towards a common erosion law for fine sand, mud and mixtures. *Water*, *9*, 564. https://doi.org/10.3390/w9080564

Merritt, W. S., Letcher, R. A., & Jakeman, A. J. (2003). A review of erosion and sediment transport models. *Environmental Modelling & Software*, *18*(8–9), 761–799. https://doi.org/10.1016/S1364-8152(03)00078-1

Migniot, C. (1968). Etude des propriétés physiques de différents sédiments très fins et de leur comportement sous des actions hydrodynamiques. *La Houille Blanche*, *7*, 591–620.

Mikes, D., Verney, R., Lafite, R., & Belorgey, M. (2004). Controlling factors in estuarine flocculation processes: Experimental results with material from the Seine Estuary, Northwestern France. *Journal of Coastal Research*, *41*, 82–89.
Morris, A. W., Mantoura, R. F. C., Bale, A. J., & Howland, R. J. M. (1978). Very low salinity regions of estuaries—Important sites for chemical and biological reactions. *Nature*, *274*(5672), 678–680. https://doi.org/10.1038/274678a0
Murray, A. B., Gasparini, N. M., Goldstein, E. B., & van der Wegen, M. (2016). Uncertainty quantification in modeling earth surface processes: More applicable for some types of models than for others. *Computers & Geosciences*, *90*, 6–16. https://doi.org/10.1016/j.cageo.2016.02.008
Panagiotopoulos, I., Voulgaris, G., & Collins, M. (1997). The influence of clay on the threshold of movement of fine sandy beds. *Coastal Engineering*, *32*(1), 19–43. https://doi.org/10.1016/S0378-3839(97)00013-6
Parra, M., Castaing, P., Jouanneau, J. M., Grousset, F., & Latouche, C. (1999). Nd-Sr isotopic composition of present-day sediments from the Gironde Estuary, its draining basins and the WestGironde mud patch (SW France). *Continental Shelf Research*, *19*(1), 135–150. https://doi.org/10.1016/S0278-4343(98)00083-1
Partheniades, E. (1965). Erosion and deposition of cohesive soils. *Journal of the Hydraulics Division*, *91*(1), 105–139.
Ridgway, J., & Shimmield, G. (2002). Estuaries as repositories of historical contamination and their impact on shelf seas. *Estuarine, Coastal and Shelf Science*, *55*(6), 903–928. https://doi.org/10.1006/ecss.2002.1035
Roberts, D. A. (2012). Causes and ecological effects of resuspended contaminated sediments (RCS) in marine environments. *Environment International*, *40*, 230–243. https://doi.org/10.1016/j.envint.2011.11.013
Roland, A., & Ardhuin, F. (2014). On the developments of spectral wave models: Numerics and parameterizations for the coastal ocean. *Ocean Dynamics*, *64*(6), 833–846. https://doi.org/10.1007/s10236-014-0711-z
Ross, L., Huguenard, K., & Sottolichio, A. (2019). Intratidal and fortnightly variability of vertical mixing in a macrotidal estuary: The Gironde. *Journal of Geophysical Research: Oceans*, *124*, 2641–2659. https://doi.org/10.1029/2018JC014456
Ross, L., Valle-Levinson, A., Sottolichio, A., & Huybrechts, N. (2017). Lateral variability of subtidal flow at the mid-reaches of a macrotidal estuary. *Journal of Geophysical Research: Oceans*, *122*, 7651–7673. https://doi.org/10.1002/2016JC012504
Roy, C. J., & Oberkampf, W. L. (2011). A comprehensive framework for verification, validation, and uncertainty quantification in scientific computing. *Computer Methods in Applied Mechanics and Engineering*, *200*(25–28), 2131–2144. https://doi.org/10.1016/j.cma.2011.03.016
Sanford, L. P. (2008). Modeling a dynamically varying mixed sediment bed with erosion, deposition, bioturbation, consolidation, and armoring. *Computers & Geosciences*, *34*(10), 1263–1283. https://doi.org/10.1016/j.cageo.2008.02.011
Savoye, N., David, V., Morisseau, F., Etcheber, H., Abril, G., Billy, I., et al. (2012). Origin and composition of particulate organic matter in a macrotidal turbid estuary: The Gironde Estuary, France. *Estuarine, Coastal and Shelf Science*, *108*, 16–28. https://doi.org/10.1016/j.ecss.2011.12.005
Schäfer, J., Blanc, G., Lapaquellerie, Y., Maillet, N., Maneux, E., & Etcheber, H. (2002). Ten-year observation of the Gironde tributary fluvial system: Fluxes of suspended matter, particulate organic carbon and cadmium. *Marine Chemistry*, *79*(3–4), 229–242. https://doi.org/10.1016/S0304-4203(02)00066-X
Schmidt, S., Ouamar, L., Cosson, B., Lebleu, P., & Derriennic, H. (2014). Monitoring turbidity as a surrogate of suspended particulate load in the Gironde Estuary: The impact of particle size on concentration estimates. I.'Paper presented at the' ISOBAY XIV International Symposium on Oceanography of the Bay of Biscay, Bordeaux,
Schulz, E., Grasso, F., Le Hir, P., Verney, R., & Thouvenin, B. (2018). Suspended sediment dynamics in the macrotidal Seine Estuary (France): 2. Numerical modeling of sediment fluxes and budgets under typical hydrological and meteorological conditions. *Journal of Geophysical Research: Oceans*, *123*, 578–600. https://doi.org/10.1002/2016JC012638
Scully, M. E., & Friedrichs, C. T. (2007). Sediment pumping by tidal asymmetry in a partially mixed estuary. *Journal of Geophysical Research*, *112*, C07028. https://doi.org/10.1029/2006JC003784
Sherwood, C. R., Aretxabaleta, A. L., Harris, C. K., Rinehimer, J. P., Verney, R., & Ferre, B. (2018). Cohesive and mixed sediment in the Regional Ocean Modeling System (ROMS v3.6) implemented in the Coupled Ocean-Atmosphere-Wave-Sediment Transport Modeling System (COAWST r1234). *Geoscientific Model Development*, *11*(5), 1849–1871. https://doi.org/10.5194/gmd-11-1849-2018
Sommerfield, C. K., & Wong, K. C. (2011). Mechanisms of sediment flux and turbidity maintenance in the Delaware Estuary. *Journal of Geophysical Research*, *116*, C01005. https://doi.org/10.1029/2010JC006462
Sottolichio, A., & Castaing, P. (1999). A synthesis on seasonal dynamics of highly-concentrated structures in the Gironde Estuary. *Comptes Rendus De L Academie Des Sciences Serie Ii Fascicule a-Sciences De La Terre Et Des Planetes*, *329*(11), 795–800. https://doi.org/10.1016/S1251-8050(00)88634-6
Sottolichio, A., Hurther, D., Gratiot, N., & Bretel, P. (2011). Acoustic turbulence measurements of near-bed suspended sediment dynamics in highly turbid waters of a macrotidal estuary. *Continental Shelf Research*, *31*(10), S36–S49. https://doi.org/10.1016/j.csr.2011.03.016
Sottolichio, A., Le Hir, P., & Castaing, P. (2000). Modeling mechanisms for the stability of the turbidity maximum in the Gironde Estuary, France. *Coastal and Estuarine Fine Sediment Processes*, *3*, 373–386. https://doi.org/10.1016/S1568-2692(00)80132-1
Soulsby, R. (1997). *Dynamics of marine sands: A manual for practical applications*. London: Thomas Telford.
Thill, A., Moustier, S., Garnier, J. M., Estournel, C., Naudin, J. J., & Bottero, J. Y. (2001). Evolution of particle size and concentration in the Rhone river mixing zone: Influence of salt flocculation. *Continental Shelf Research*, *21*(18–19), 2127–2140. https://doi.org/10.1016/S0278-4343(01)00047-4
Thorn, M., & Parsons, J. (1980). Erosion of cohesive sediments in estuaries: An engineering guide. I. Paper presented at the Proc. of the Int. Symp. on Dredging Technol,
Uncles, R. J., Elliott, R. C. A., & Weston, S. A. (1985). Observed fluxes of water, salt and suspended sediment in a partly mixed estuary. *Estuarine, Coastal and Shelf Science*, *20*(2), 147–167. https://doi.org/10.1016/0272-7714(85)90035-6
Underwood, G. J. C., & Kromkamp, J. (1999). Primary production by phytoplankton and microphytobenthos in estuaries. *Advances in Ecological Research*, *29*, 93–153. https://doi.org/10.1016/S0065-2504(08)60192-0
van Kessel, T., Vanlede, J., & de Kok, J. (2011). Development of a mud transport model for the Scheldt Estuary. *Continental Shelf Research*, *31*(10), S165–S181. https://doi.org/10.1016/j.csr.2010.12.006
van Ledden, M., van Kesteren, W. G. M., & Winterwerp, J. C. (2004). A conceptual framework for the erosion behaviour of sand-mud mixtures. *Continental Shelf Research*, *24*(1), 1–11. https://doi.org/10.1016/j.csr.2003.09.002
van Leussen, W. (1994). *Estuarine macroflocs and their role in fine-grained sediment transport*. Utrecht: I. University of Utrecht.
van Maanen, B., & Sottolichio, A. (2018). Hydro- and sediment dynamics in the Gironde Estuary (France): Sensitivi to seasonal variations in river inflow and sea level rise. *Continental Shelf Research*, *165*, 37–50. https://doi.org/10.1016/j.csr.2018.06.001

van Maren, D. S., & Cronin, K. (2016). Uncertainty in complex three-dimensional sediment transport models: Equifinality in a model application of the Ems Estuary, the Netherlands. *Ocean Dynamics*, *66*(12), 1665–1679. https://doi.org/10.1007/s10236-016-1000-9

van Rijn, L. C. (1984). Sediment pick-up functions. *Journal of Hydraulic Engineering-Asce*, *110*(10), 1494–1502. https://doi.org/10.1061/(ASCE)0733-9429(1984)110:10(1494)

van Rijn, L. C., Bisschop, R., & van Rhee, C. (2019). Modified sediment pick-up function. *Journal of Hydraulic Engineering*, *145*(1), 06018017. https://doi.org/10.1061/(ASCE)HY.1943-7900.0001549

Viney, N. R., & Sivapalan, M. (1999). A conceptual model of sediment transport: Application to the Avon River basin in Western Australia. *Hydrological Processes*, *13*(5), 727–743. https://doi.org/10.1002/(SICI)1099-1085(19990415)13:5<727::AID-HYP776>3.0.CO;2-D

Waeles, B., Le Hir, P., & Lesueur, P. (2008). A 3D morphodynamic process-based modelling of a mixed sand/mud coastal environment: The Seine Estuary, France. In T. Kusuda, H. Yamanishi, J. Spearman, & J. Z. Gailani (Eds.), *Sediment and Ecohydraulics: INTERCOH2005, Proceedings in Marine Science* (Vol. 9, pp. 477–498). Elsevier. https://doi.org/10.1016/S1568-2692(08)80034-4

Waeles, B., Le Hir, P., Lesueur, P., & Delsinne, N. (2007). Modelling sand/mud transport and morphodynamics in the Seine River mouth (France): An attempt using a process-based approach. *Hydrobiologia*, *588*(1), 69–82. https://doi.org/10.1007/s10750-007-0653-2

Winterwerp, J. C., Zhou, Z., Battista, G., Van Kessel, T., Jagers, H. R. A., Van Maren, D. S., & Van der Wegen, M. (2018). Efficient consolidation model for morphodynamic simulations in low-SPM environments. *Journal of Hydraulic Engineering*, *144*, 04018055. https://doi.org/10.1061/(ASCE)HY.1943-7900.0001477

Wischmeier, W. H., & Smith, D. D. (1978). Predicting rainfall erosion losses—A guide to conservation planning. Predicting Rainfall Erosion Losses-a Guide to Conservation Planning.